AGU PUBLICATIONS

JGR

Journal of Geophysical Research: Atmospheres

RESEARCH ARTICLE
10.1002/2017JD026534

Key Points:
- NH_3 mixing ratios between 0 and 280 m altitude increase toward the surface with greater variability during the daytime than at night
- The surface at this site can act as either a source or sink of NH_3, depending on factors including temperature and source region
- Diurnal trends at higher altitudes appear to be driven by transport, while at lower altitudes, the impact of surface emissions and boundary layer height are important

Supporting Information:
- Supporting Information S1

Correspondence to:
J. G. Murphy,
jmurphy@chem.utoronto.ca

Citation:
Tevlin, A. G., Li, Y., Collett, J. L., McDuffie, E. E., Fischer, E. V., & Murphy, J. G. (2017). Tall tower vertical profiles and diurnal trends of ammonia in the Colorado Front Range. *Journal of Geophysical Research: Atmospheres*, *122*, 12,468–12,487. https://doi.org/10.1002/2017JD026534

Received 20 JAN 2017
Accepted 29 OCT 2017
Accepted article online 3 NOV 2017
Published online 22 NOV 2017

Tall Tower Vertical Profiles and Diurnal Trends of Ammonia in the Colorado Front Range

A. G. Tevlin[1], Y. Li[2], J. L. Collett[3], E. E. McDuffie[4,5,6], E. V. Fischer[3], and J. G. Murphy[1]

[1]Department of Chemistry, University of Toronto, Toronto, Ontario, Canada, [2]Air Quality Division, Arizona Department of Environmental Quality, Phoenix, AZ, USA, [3]Department of Atmospheric Science, Colorado State University, Fort Collins, CO, USA, [4]Cooperative Institute for Research in Environmental Sciences, University of Colorado Boulder, Boulder, CO, USA, [5]Chemical Sciences Division, Earth System Research Laboratory, NOAA, Boulder, CO, USA, [6]Department of Chemistry, University of Colorado Boulder, Boulder, CO, USA

Abstract Ammonia (NH_3) mixing ratios were measured between the surface and 280 m aboveground level from a moveable carriage at the Boulder Atmospheric Observatory tower in summer 2014 as part of the Front Range Air Pollution and Photochemistry Éxperiment. The campaign median mixing ratio was 3.3 ppb, ranging from below detection limits to 192 ppb. Median vertical profiles show an overall increase in NH_3 mixing ratios toward the surface of 6.7 ppb (89%) during the day and 3.9 ppb (141%) at night. In contrast to the overall increasing trend, some individual profiles show decreasing NH_3 in the lowest 10 m. This suggests that the local surface is capable of acting as either a source or a sink, depending on the relative amounts of NH_3 at the surface, and in advected air parcels. We further use this data set to investigate the variation in diurnal patterns of NH_3 as a function of height above the surface. At higher altitudes (100 ± 5 and 280 ± 5 m), NH_3 mixing ratios reach a gradual maximum during the day between 9:00 and 16:00 local time, likely driven by changes in source region. At lower altitudes (10 ± 5 m), the daytime maximum begins earlier at about 7:00 local time, followed by a sharper increase at 9:00 local time. At this height we also observe a peak in NH_3 mixing ratios during the night, likely driven by the trapping of emitted NH_3 within the shallower nocturnal boundary layer.

Plain Language Summary Atmospheric ammonia has wide ranging impacts on environmental and human health. Although it has strong sources and sinks at the earth's surface, not many studies have investigated the way that its concentration changes with altitude in the first few hundred meters above the ground. Here we present ammonia measurements made from a tall tower showing changes in ammonia concentration with height and the way that these changes can differ throughout the hours of the day. This information can be important to better understand the processes that impact ammonia concentrations and to improve our ability to represent these processes in models.

1. Introduction

As the dominant atmospheric base, ammonia (NH_3) plays an important role in the formation and neutralization of aerosols, which can impact human health, atmospheric visibility, and the global radiation budget (Adams et al., 2001; Aneja, Schlesinger, & Erisman, 2009; Barthelmie & Pryor, 1998; Henze et al., 2012; Pinder et al., 2012). It is also a significant contributor to nitrogen deposition, which can have negative impacts on ecosystems (Erisman et al., 2007; Fenn et al., 2003; Krupa, 2003; Phoenix et al., 2012). Despite this, measurements of gaseous NH_3 are lacking. In particular, there are few long-term measurements at a high temporal resolution and very little information available on the near-surface vertical distribution of NH_3 mixing ratios extending further than a few meters away from the surface (Erisman et al., 1988; Ryden & Mcneill, 1984). As a trace gas with both point and area-wide surface sources, as well as a tendency to deposit rapidly to surfaces, NH_3 mixing ratios can be expected to vary significantly as a function of altitude. A greater understanding of its vertical distribution is especially important given recent advances in satellite retrievals, which offer great potential for understanding the global distribution of gaseous NH_3. These retrievals are less sensitive toward the surface and depend heavily on a priori profiles of NH_3 mixing ratios throughout the lowest layers of the atmosphere; they also require information on the distribution of NH_3 for retrieval validation (Shephard & Cady-Pereira, 2015; Sun et al., 2015; Van Damme et al., 2015).

Both the surface exchange and gas-particle partitioning of NH_3 have been shown to depend heavily on changes in meteorological conditions, including temperature, relative humidity, and wind speed (Hensen et al., 2009;

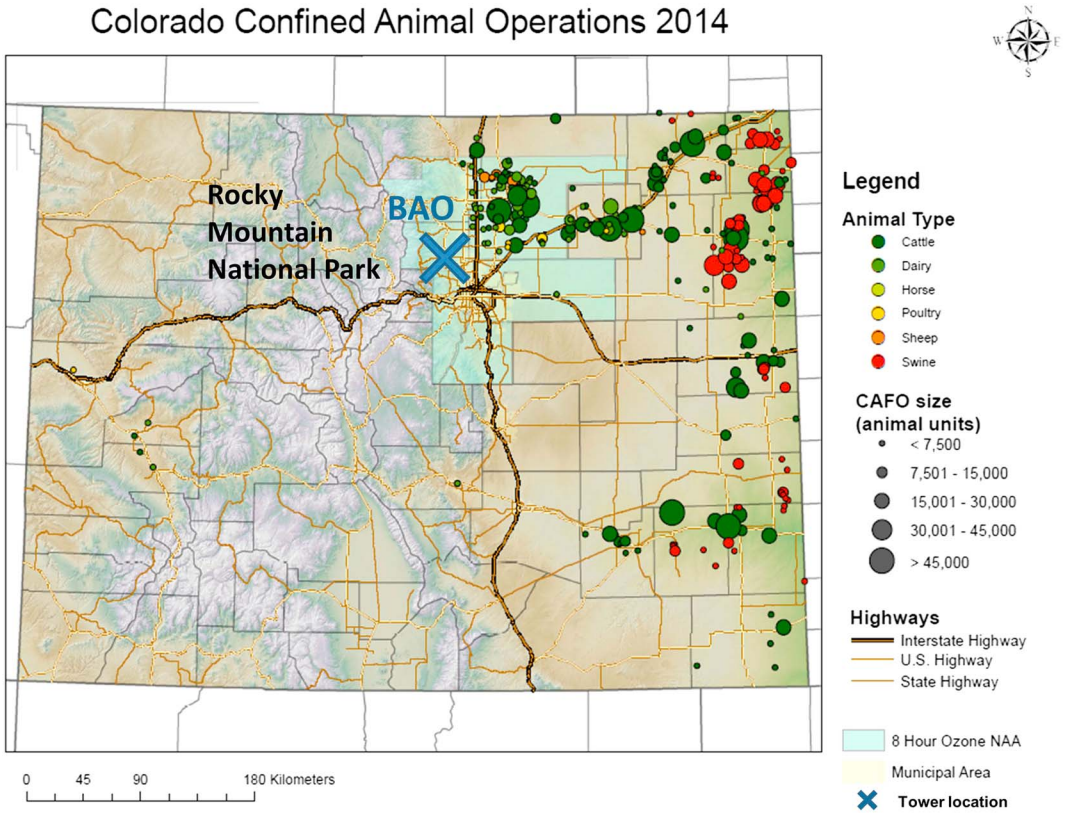

Figure 1. Map of the Colorado Front Range showing the location of the measurement tower and of nearby Concentrated Animal Feeding Operations (CAFOs). Livestock census data come from the Colorado Department of Public Health and Environment, (CDPHE), compiled by the Air Pollution Control Division (APCD) staff. The light blue color shows the 8 h ozone nonattainment area.

Sommer, Olesen, & Christensen, 2009; Stelson & Seinfeld, 2007; Zhang, Wright, & Asman, 2010). NH_3 emissions over strong sources such as hog waste storage lagoons have been seen to depend exponentially on temperature because of the impacts of temperature on liquid mass transfer and solubility (Aneja, Chauhan, & Walker, 2000). Greater wind speeds have also been seen to increase emissions (Sommer, Christensen, & Nielsen, 1993). Surfaces with low NH_3 content can also act as NH_3 sinks through deposition. In areas where ambient NH_3 mixing ratios are similar to the equilibrium value that would be expected over the surface, bidirectional exchange can take place, with the direction and magnitude of the exchange additionally depending on meteorological factors such as temperature and atmospheric turbulence (Zhang et al., 2010). Some of the resulting variability in NH_3 mixing ratios is fairly well understood. On an annual scale, for example, NH_3 mixing ratios typically exhibit a maximum in warmer months due to increased emissions as well as conditions that do not favor partitioning to particle NH_4^+ (Li et al., 2014; Meng et al., 2011; Walker et al., 2004). Diurnal cycles in NH_3 mixing ratios are somewhat more complex and can differ greatly depending on the location of measurements and the strength and proximity of emission sources (Chen et al., 2014; Erisman et al., 2001; Pinder et al., 2011; Saylor et al., 2010). This complexity is highlighted by the difficulty that many models have in capturing these diurnal cycles (Asman & van Jaarsveld, 1992; Markovic et al., 2014; Zhu et al., 2015). Additionally, there is little existing information on changes in diurnal trends of NH_3 with altitude, information that can help to illuminate some of the different drivers of these trends (Lonsdale et al., 2016).

The Colorado Front Range is an interesting region in terms of air quality because of its various emission sources, as well as the meteorology of the region (Brown et al., 2013; Haagenson, 1979). The primary sources of NH_3 in this region are agricultural, the result of a high density of Concentrated Animal Feeding Operations (CAFOs) including cattle, dairy, and hog operations, ranging in size from less than 7,500 to more than 45,000 animals (Figure 1). Other sources of NH_3 include agricultural fertilizer use (Goebes, Strader, & Davidson, 2003),

traffic (Moeckli, Fierz, & Sigrist, 1996; Watson et al., 1998), and urban emissions from throughout the Northern Front Range Metropolitan Area, encompassing the cities of Denver, Boulder, Longmont, Greeley, and Fort Collins (Nowak et al., 2012). In contrast, Rocky Mountain National Park, situated to the west, contains few sources of NH_3 and is more likely to act as a sink than as a source for NH_3 (Benedict et al., 2013; Gebhart et al., 2011). A few studies have investigated surface level NH_3 mixing ratios in this region; however, none of these describes the vertical changes in NH_3 with the level of spatial and temporal resolution achieved here. Measured mixing ratios were found to vary greatly between sites, but mixing ratios in the summer tended to range between 4 and 11 ppb (Day et al., 2012; Heald et al., 2012 ; Watson et al., 1998). As expected, NH_3 mixing ratios in northeastern Colorado have been found to be higher in the warmer summer months, but a slight increase in wintertime NH_3 as compared to fall and spring has also been observed (Day et al., 2012). This was attributed to the trapping of emissions within a shallower and less well-ventilated winter boundary layer.

Given the propensity of total NH_3 to partition between the gas and particle phase, it is also useful to know how much particle NH_4^+ is available to influence gas phase mixing ratios through partitioning. The formation of $(NH_4)_2SO_4$ is essentially irreversible, meaning that SO_4^{2-} particles can act as an NH_3 sink, but meteorology will have a weaker influence on gas-particle partitioning compared to NH_4NO_3, which is semivolatile (Seinfeld & Pandis, 2006). Measurements of particle NO_3^- may therefore provide a better estimate of how much particle NH_4^+ might influence gas-phase NH_3 mixing ratios, rather than particle NH_4^+ itself. Existing analyses based on measurements and chemical transport modeling indicate that the region is NH_3-rich, with the formation of NH_4NO_3 particles being limited by HNO_3 rather than NH_3 (Heald et al., 2012; Watson et al., 1998). Concentrations of particle NO_3^- in the Colorado Front Range in August have previously been measured in the range of 0.5–1.25 $\mu g/m^3$ (Day et al., 2012; Heald et al., 2012). Taking 1 $\mu g/m^3$ as an average value, this shows that particulate NH_4NO_3 could only contribute about 0.3 ppb to gas-phase NH_3 mixing ratios. NO_3^- measurements from this campaign will be discussed in section 3.1.

The National Science Foundation Front Range Air Pollution and Photochemistry Éxperiment (FRAPPÉ) campaign was a large collaborative effort involving aircraft, mobile, and stationary ground measurements of many different species of interest to air quality in the Colorado Front Range. This campaign included the installation of several instruments inside the Portable Instrument Shelter with Amenities (PISA) mounted on the outside moveable carriage attached to the Boulder Atmospheric Observatory (BAO) tower in Erie Colorado, enabling the measurement of vertical profiles of atmospheric components over a range up to 280 m in altitude without the use of long inlet tubing (Brown et al., 2013). From this platform, a Quantum Cascade-Tunable Infrared Laser Differential Absorption Spectrometer (QC-TILDAS) was deployed with the goal of elucidating the near-surface vertical profiles of NH_3 mixing ratios and the diurnal changes in this profile. The resulting data set allowed us to investigate the impacts of some of the factors that drive these trends, including bidirectional surface-atmosphere exchange, horizontal advection, boundary layer dilution, and gas-particle partitioning.

2. Methods

2.1. Site Details

The BAO tower is located in Erie, Colorado (40 03 00.10028 N, 105 00 13.80781 W), about 20 km to the northeast of Boulder (Kaimal & Gaynor, 1983). Figure 1 shows the location of the site, as well as the locations of nearby CAFOs, which contribute to the heterogeneous source region. The local surface around the site consists of approximately 5,000 m^2 of bare earth with a number of trailers containing instrumentation, surrounded by a 0.5 km^2 short grass field. The 300 m tower has a number of meteorological sensors at multiple altitudes. The mixed layer height was determined every 6 s by a Vaisala CL51 ceilometer capable of profiling between 0 and 15 km using backscattered LIDAR (Knepp et al., 2017). The tower is outfitted with a moveable instrument carriage (PISA) able to carry an instrument payload of up to 772 kg, while making a full ascent or descent approximately every 15 min. Due to different operational requirements of instruments on board the carriage during the campaign, there were limitations on the number and timing of ascents, and the carriage was frequently kept stationary at one of several heights for extended periods. In total, 241 full or partial profiles of vertical NH_3 mixing ratio were obtained, including several periods of continuous profiling. The instrumentation trailers have the potential to influence wind direction and turbulent transport, as does the presence of the tower itself on the northeast side of the carriage. In order to minimize artifacts in NH_3

mixing ratios, data were filtered before analysis to remove times when the carriage was brought to the ground for instrument maintenance. All data are presented in local time (MDT = UTC 6:00).

2.2. Instrument Details

The QC-TILDAS (Aerodyne Research Inc.) used in this study measures NH_3 mixing ratios using an absorption feature at 967 cm^{-1} (McManus et al., 2008). Instrument precision varied throughout the campaign depending on operating conditions, with an estimated 3σ limit of detection of 0.5 ppb at a sampling rate of 1 Hz. Background spectra were obtained every half hour during the campaign using NH_3-free air generated by a palladium catalyst heated to 360°C (Aadco Instruments). This catalytic technique for NH_3 removal has been used successfully in other studies (e.g., Norman, Hansel, & Wisthaler, 2007), and we confirmed prior to the campaign that it effectively removed NH_3 while maintaining a relative humidity close to that of ambient air. Instrument software divided raw ambient spectra by these background spectra before fitting the absorption peaks and calculating mixing ratios. Imperfections in the modeled fit of measured spectra cause inaccuracies in calculated values; however, these have been shown to be stable over a wide range of mixing ratios and can therefore be reliably corrected by calibration (Ellis et al., 2010). This was achieved by periodically introducing 1.7 ppb NH_3 from a permeation source (KIN-TEK Laboratories, Inc.). In order to obtain adequate calibrations while minimizing the interruptions to data collection, calibrations were run approximately every 72 h. Multiplicative correction factors were interpolated between these points and can be seen in Figure S1 in the supporting information. Based on the variability in the backgrounds and calibrations, the accuracy of the ambient measurements is estimated to be 20% + 0.5 ppb. In order to avoid artifacts from the volatilization of particle NH_3 in the form of NH_4NO_3, as well as to protect the optical system from damage, it is important to remove particulate matter from the sample stream. In order to improve time response and reduce artifacts, the QC-TILDAS is equipped with a quartz virtual impactor inlet with a fluorinated silane coating that removes particles without the use of a filter (Ellis et al., 2010). Additionally, the length of the inlet tubing (PFA, I.D. 3/8″) was kept as short as possible (3 m), and both the inlet and tubing were heated to approximately 40°C.

The carriage also contained several other analytical instruments, including a Picarro 2401 cavity ringdown trace gas analyzer that provided CH_4 and CO mixing ratios (5 s precision $<$1 ppb and $<$15 ppb and maximum uncertainty $<$1 ppb and $<$2 ppb for CH_4 and CO, respectively). We also compare our results to NH_3 measurements by a proton transfer-time of flight mass spectrometer (PT-ToF-MS) onboard the NASA P3 aircraft (1 Hz LOD: 0.38 ppb), another QC-TILDAS aboard the C-130 aircraft (uncertainty: ±(28% + 0.328 ppb) + 0.111 ppb and an open path QCL-based NH_3 sensor mounted on a ground-based vehicle (1 s precision: 0.15 ppb, uncertainty: 0.20 ppb ± 10%) (Miller et al., 2014; Müller et al., 2014). Finally, particle speciation measurements were made aboard the P3 aircraft by Particle Into Liquid Sampler-Ion Chromatography (PILS-IC) (uncertainty: 20%) (Beyersdorf et al., 2016). The PILS-IC, open-path, and PT-ToF-MS measurements were made during the complementary National Aeronautics and Space Administration Deriving Information on Surface Conditions from COlumn and VERtically Resolved Observations Relevant to Air Quality field study at the same time and over the same region.

2.3. Data Analysis Details

Data analysis took one of two forms. First (method 1), full vertical profiles were examined, using only data from periods during which the carriage was ascending or descending and excluding periods when the carriage was stationary in order to avoid biasing results toward any one height. These 1 Hz NH_3 mixing ratio profiles were separated into 10 m vertical bins to calculate median profiles and variability. For comparisons between nighttime and daytime profiles, night and day were defined as the periods from 21:00 to 3:00 and 9:00 to 15:00, respectively, excluding the transitional periods between these two states (all times are given in local time, MDT). This choice highlights the contrast between the stable well-established low boundary layer nighttime conditions and the well-mixed daytime column (Riedel et al., 2013). Second (method 2), data were filtered for time periods when the carriage was within 5 m of three different heights: 10 m, 100 m, and 280 m. These specific heights were chosen to coincide with the locations of meteorological stations on the tower. Method 2 takes advantage of the greater quantity of data gathered while the carriage was stationary and simplifies the vertical dimension for the purposes of investigating diurnal patterns.

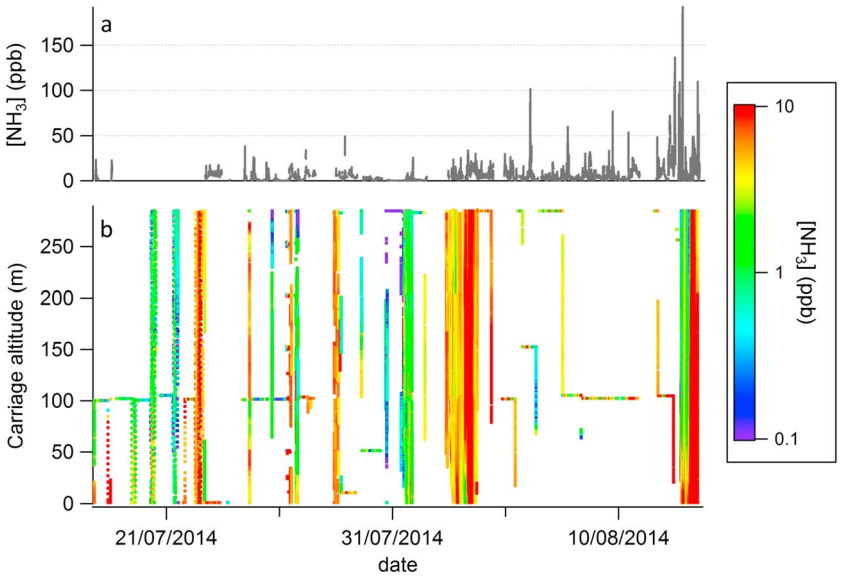

Figure 2. (a) Time series of 1 Hz NH_3 mixing ratio throughout the campaign. (b) Carriage altitude throughout the campaign at 1 Hz, colored by measured NH_3 mixing ratio (note that color bar is on a log scale and that values above the color scale maximum have been set to the maximum color, while values below the minimum have been set to the minimum color).

3. Data and Interpretation

NH_3 mixing ratios measured over the full campaign (17 July to 13 August 2014) are shown in Figure 2a. Mixing ratios range from below detection limit (<0.5 ppb) to as high as 192 ppb, with a mean and standard deviation of 5.5 ± 7.7 ppb and a median of 3.3 ppb across the entire campaign, which is within the range of other measurements made in this region (Day et al., 2012; Heald et al., 2012; Li et al., 2016; Watson et al., 1998). Source region is one of the major drivers of the high variability seen in the NH_3 mixing ratios measured here. This is demonstrated in Figure 3a, which reflects the impact of the heterogeneous emission sources surrounding the measurement site throughout the campaign. The highest mixing ratios are observed when the wind arrives from the north and east, where the majority of CAFOs are located. In contrast, the lowest mixing ratios are observed during westerly and southwesterly winds coming from the direction of the Rocky Mountains and

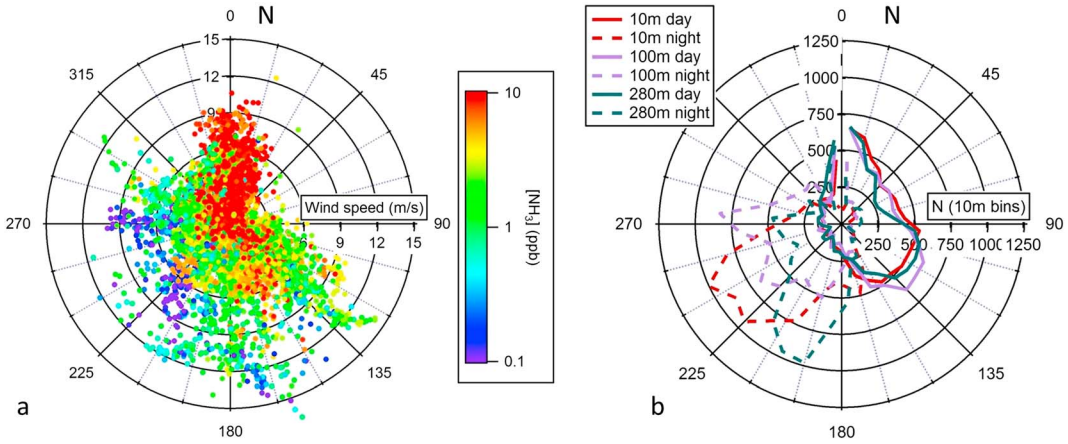

Figure 3. (a) NH_3 mixing ratio dependence on wind direction. Radial data are wind speed as a function of wind direction, colored by NH_3 mixing ratio (note that color is on a log scale and that values above the color scale maximum have been set to the maximum color, while values below the minimum have been set to the minimum color). (b) Wind direction at three heights during the day (9:00–15:00 MDT) and night (21:00–3:00 MDT). Radial scale shows frequency of wind direction in terms of counts within 10° bins.

the city of Boulder. The presence of higher mixing ratios of NH_3 to the north and east of the site was confirmed by mobile measurement platforms (both aircraft and ground vehicles) involved in the campaign (see Figure S2). Comparison with other coemitted trace gases can help to elucidate the sources of this NH_3. Emissions from agriculture, for example, can be expected to have a distinct ratio of NH_3 to CH_4, whereas traffic emissions can be expected to have a distinct ratio of NH_3 to CO_2. In order to improve the sensitivity of this comparison, it can be helpful to look at the ratio of excess values of each species rather than their absolute values. Excess values are defined here as mixing ratios above a set background value, where the background value is taken to be the minimum value within a running window, the length of which is determined using an optimization algorithm as described in Atherton et al. (2017). Eilerman et al. (2016) compiled excess NH_3/CH_4 ratios (eNH_3:eCH_4) from several studies, including the FRAPPE campaign, showing that ratios from a variety of agricultural sources fall between 100 and 1,000 (mmol/mol). Similarly, excess ratios of NH_3 to CO_2 (eNH_3:eCO_2) between approximately 0.1 and 0.75 (mmol/mol) can be indicative of traffic sources of NH_3 (Sun et al., 2014; Sun et al., 2017). Throughout the campaign, 67% of measurements fell within an agricultural range of eNH_3:eCH_4, while 28% of measurements fell within a traffic-derived range of eNH_3:eCO_2. Neither of these source indicators, however, shows the strong dependence on wind direction seen in the absolute NH_3 mixing ratio (Figure S3).

The difference between the emission rates from these different source regions is expected to be enhanced during the daytime, as higher temperature and wind speeds increase the emission rate of NH_3 from the nearby CAFOs (Eilerman et al., 2016). The distribution of daytime and nighttime wind directions at the three tower heights used in method 2 is shown in Figure 3b. While the overall wind direction is similar at all three altitudes, it differs greatly between night and day. During the night (21:00 to 3:00 MDT) air at the site tends to arrive from the southwest, driven by downslope flow, while during the day, it arrives more frequently from directions that range between the north and southeast. Despite the apparent lack of wind from the northeast, likely caused by airflow disturbance from the tower to the northeast of the carriage, for simplicity, we will refer to this wide range as centering on the northeast. This meteorological pattern of upslope and downslope flow causing nighttime winds from the southwest and daytime winds from a range centering around the northeast has been observed during other campaigns at this location (Brown et al., 2013; Neff, 2016; Toth, Toth, & Johnson, 1984), and its impact on diurnal patterns will be discussed in section 3.2.

A number of factors complicate the analysis of this data set, including the heterogeneity of regional NH_3 sources seen in Figure 1. The inclusion of the vertical dimension adds a further source of complexity to the time series, especially given that the changing measurement height (at a rate of approximately 0.4 m s^{-1}) changes the size of the footprint from which the influence of surface exchange can be expected, with footprint size and the distance of the area of maximum flux both increasing along with receptor height (Kljun et al., 2015). Nevertheless, two primary observations have been made. First, the mixing ratio of NH_3 increases significantly toward the surface over a relatively small ($<$300 m) vertical range. While this is not surprising, this is the first report of continuous measurements of NH_3 mixing ratios within this range of the atmosphere with this degree of spatial and temporal resolutions. There is a large amount of variability between individual profiles, but the lower variability overnight allows the near-surface increase to be more evident than during the day. Second, diurnal profiles of NH_3 vary with measurement height. Small daytime maxima were observed at 100 m and 280 m, while measurements at 10 m displayed a more extreme daytime increase (up to 15 ppb) as well as an overnight increase (up to 10 ppb). Each of these observations is discussed in turn below.

3.1. Vertical Profiles

Figure 2b presents vertical profiles measured over the full campaign colored by NH_3 mixing ratio. Expansions of two intensive profiling periods can be seen in Figure S4, highlighting the detailed vertical information available in this data set. Median vertical profiles (method 1) along with the 10th, 25th, 75th, and 90th percentiles are shown in Figure 4 for the full data set, as well as for isolated night and day periods. Corresponding profiles of temperature, relative humidity, and wind speed during the night and day are provided in Figure S5. The 13.4 ppb interquartile range in Figure 4a indicates that the variation between individual profiles is quite high relative to median values (between 3.3 and 6.6 ppb). When every profile is included (Figure 4a) there is a 2.7 ppb (66%) increase in mixing ratio toward the surface. The median column mixing ratio during the daytime (Figure 4b) is 4.7 ppb higher than at night (Figure 4c), and the absolute increase toward the surface is 2.7 ppb stronger. These daytime increases are observed even when the top of the

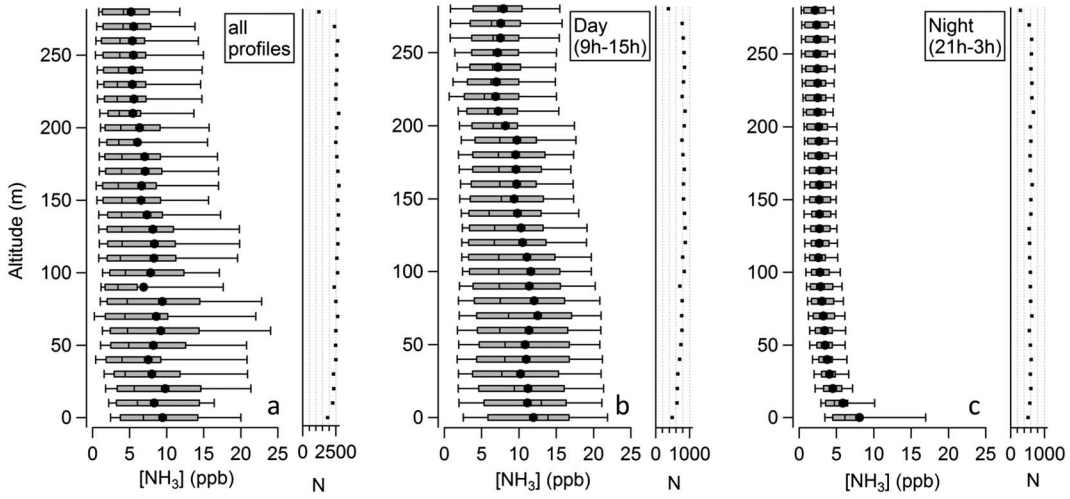

Figure 4. NH_3 binned by altitude (a) over 24 h of each day, (b) during the day (9:00–15:00), and (c) during the night (21:00–3:00). The lines and dots represent the median and mean, respectively. The shaded boxes show the 75th and 25th percentiles, while the whiskers represent the 90th and 10th percentiles. Also shown are the number of data points contained in each 10 m vertical bin (*N*). Note the difference in scale for *N* in each panel.

boundary layer is above 280 m, and measurements might be assumed to be within a well-mixed boundary layer. In contrast, the relative increase is higher at night (141% compared to 89%), and the lower variability (both absolute and relative) throughout the column causes this trend to be more evident.

Measurements of NH_3 by a PTR-TOF-MS aboard the NASA P-3 aircraft and a QC-TILDAS aboard the C-130 aircraft restricted to an area of 10 km^2 around the BAO tower show that this decreasing trend continues at higher altitudes. In Figure 5, NH_3 mixing ratios from these measurements are plotted as a function of altitude in the same way as Figure 4, binned instead by 100 m. NH_3 mixing ratios measured within the bottom three 100 m bins by the QC-TILDAS on the aircraft (Figure 5b) agree fairly well with those measured from the tower during the daytime (Figure 4b). Those measured by the PTR-TOF-MS (Figure 5a) are somewhat lower;

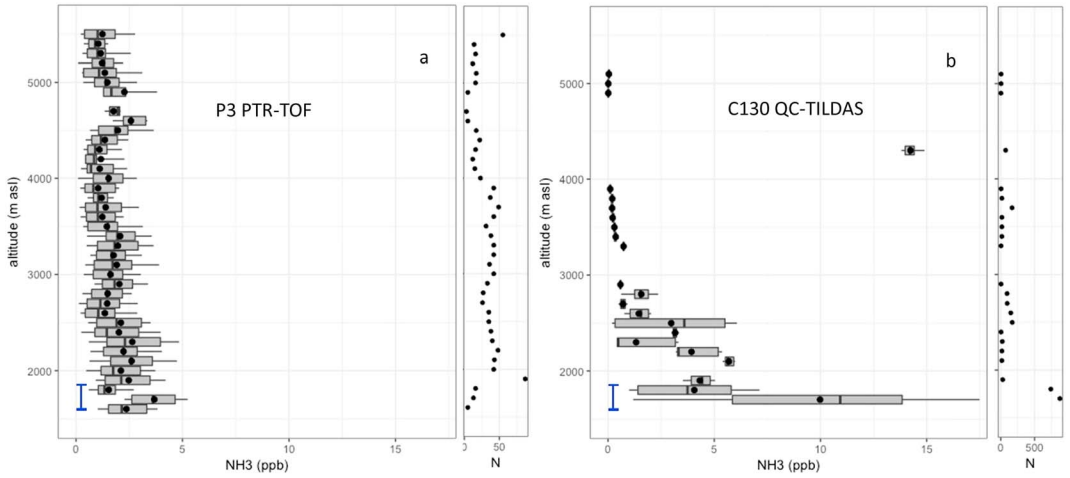

Figure 5. NH_3 measured (a) by PTR-TOF-MS aboard the NASA P3 aircraft and (b) by QC-TILDAS aboard the C-130 aircraft. Data are shown from daytime periods when either aircraft was within a 10 km^2 area around the BAO tower. In the case of the PTR-TOF-MS this consists of four spirals above the tower, while in the case of the QC-TILDAS, this consists of a number of transects through the area. Data are binned by altitude, where the lines and dots represent the median and mean, respectively. The shaded boxes show the 75th and 25th percentiles, while the whiskers represent the 90th and 10th percentiles. The blue bars on each plot show the altitude range of the tower in m ASL. Also shown are the number of data points contained in each 100 m vertical bin (*N*).

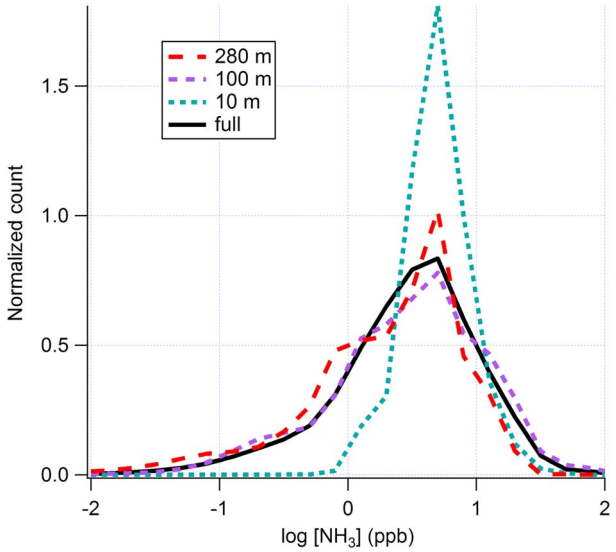

Figure 6. Histogram (normalized to unit area) of NH_3 mixing ratios measured during periods when the carriage was stationary over the full campaign (black trace) and at three different heights (red, purple, and cyan traces). Negative mixing ratios made up <3% of data points and have been omitted here.

however, the range of variability overlaps with that from the tower. Since there are relatively few data points within these lowest PTR-TOF bins, it may be that they were sampled at a time when the highly variable NH_3 mixing ratios were lower than average.

The increase in NH_3 toward the ground (Figures 4 and 5) indicates that the local surface can act as an NH_3 source. The importance of this source is also reflected in Figure 6, which shows a histogram of observed NH_3 mixing ratios at three heights: 10, 100, and 280 m. While the highest average mixing ratio is found at 100 m, measurements at 10 m show the fewest near-zero values when compared to 100 and 280 m. Given the similarity in wind direction throughout the column (Figure 3b), this suggests that bidirectional exchange with the surface plays a role in maintaining NH_3 mixing ratios at 10 m as opposed to 100 and 280 m, which are at a greater distance from this process. The decrease in NH_3 away from the surface can likely be explained both by the limitations of vertical mixing on the transport of these higher mixing ratios throughout the mixed layer as well as the periodic isolation of higher altitudes from the surface due to occasional low boundary layer heights. This is particularly evident in the night (Figure 4c) when near-surface wind speeds drop dramatically (Figure S5), reducing turbulent transport to higher altitudes, and low mixed layer heights (Figure S6) separate the surface-impacted volume from the rest of the column.

Given the complexity of the relationship between mixing ratios and meteorological variables in this data set, as well as the high degree of variability, it may be useful to examine some individual profiles that highlight these two processes. Figure 7 provides example daytime and nighttime profiles with corresponding profiles in meteorological variables. A detailed inspection of an individual nighttime profile (Figure 7a) highlights the lower variability and clear surface increase typical of nighttime profiles, as observed in Figure 4c. Throughout this profile, winds arrive consistently from the north, eliminating wind direction as an explanation for the surface increase. Wind speed and temperature decrease toward the surface from an altitude of approximately 70 m. However, the increase in NH_3 mixing ratio, similarly to that of relative humidity, begins at a lower altitude than the boundary layer height indicated by the measured temperature inversion. Two things may have contributed to the observed profile: (1) weak turbulent transport due to low nighttime wind speeds and (2) isolation of the surface from higher altitudes due to the reduced nocturnal boundary layer height. In order to highlight the impact of the boundary layer separation on the vertical distribution of NH_3, Figure 8 shows the carriage trajectory as it passes through the boundary layer. As it moves above the surface mixed layer (at 8:30 and 9:30 MDT), the mixing ratios of NH_3 can be seen to drop. This demonstrates the limitations on vertical NH_3 transport caused by the isolation of higher altitudes from the surface source contained within a shallow mixed layer.

Overnight NH_3 mixing ratios are most variable in the lowest vertical bin, where surface partitioning can exert the strongest influence (Figure 4c). During the day, variability exists more uniformly throughout the column, with much of this variability driven by changes in source region (Figure 4b). Figure 7b shows that abrupt changes in the abundance of NH_3 can occur throughout a given profile, often related to changes in wind direction. The lack of structure in the temperature profile suggests that the top of the boundary layer is located above the highest altitude of the BAO tower during the time this profile was collected, and neither NH_3 mixing ratios nor meteorological variables exhibit clear altitude dependency. The slight increase in mixing ratio toward the surface observed in Figure 4b, however, indicates that the influence of the surface persists during the day despite more thorough boundary layer mixing.

Surfaces can act either as sources or sinks of NH_3, depending on surface NH_3 content, ambient NH_3 mixing ratios, and local meteorology (Zhang et al., 2010). While many individual nighttime profiles (e.g., Figure 7a) show the continuous increase toward the surface observed in the median profile (Figure 4c), a number of profiles exhibit a small decrease in NH_3 mixing ratios immediately above the surface (e.g., Figure 7c). These profiles likely indicate periodic deposition of NH_3 to the surface, as has been observed previously at this

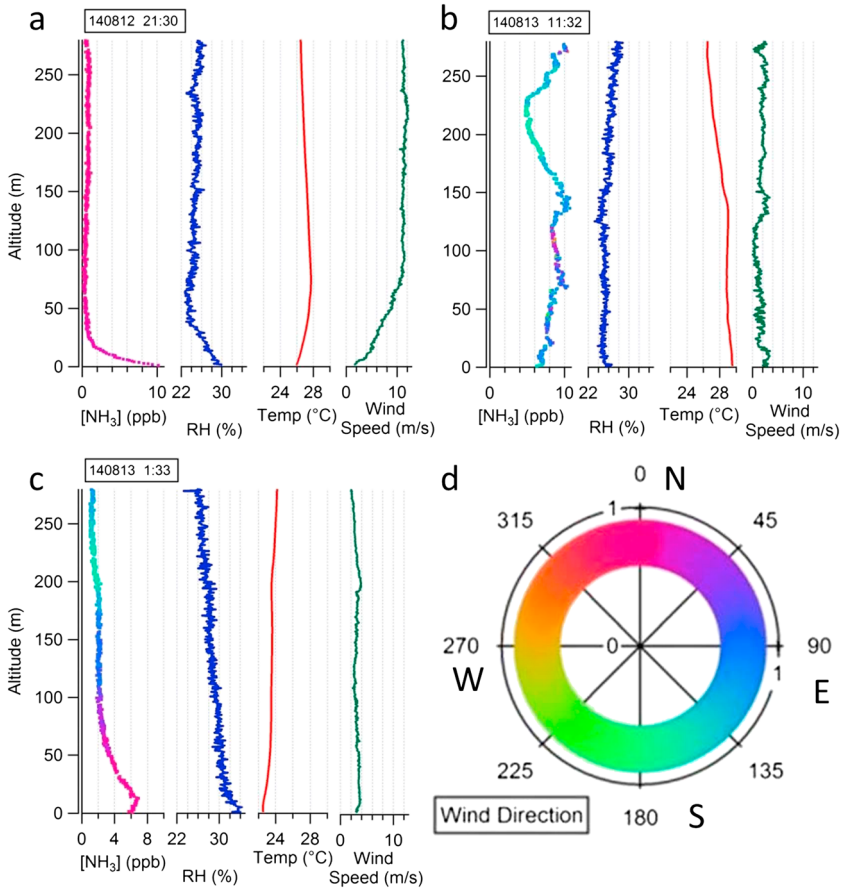

Figure 7. (a–c) Three individual vertical profiles of NH_3 mixing ratio are shown, colored by (d) wind direction. Individual vertical profiles of associated meteorological variables (relative humidity, temperature, and wind speed) are also shown for each of the three NH_3 profiles.

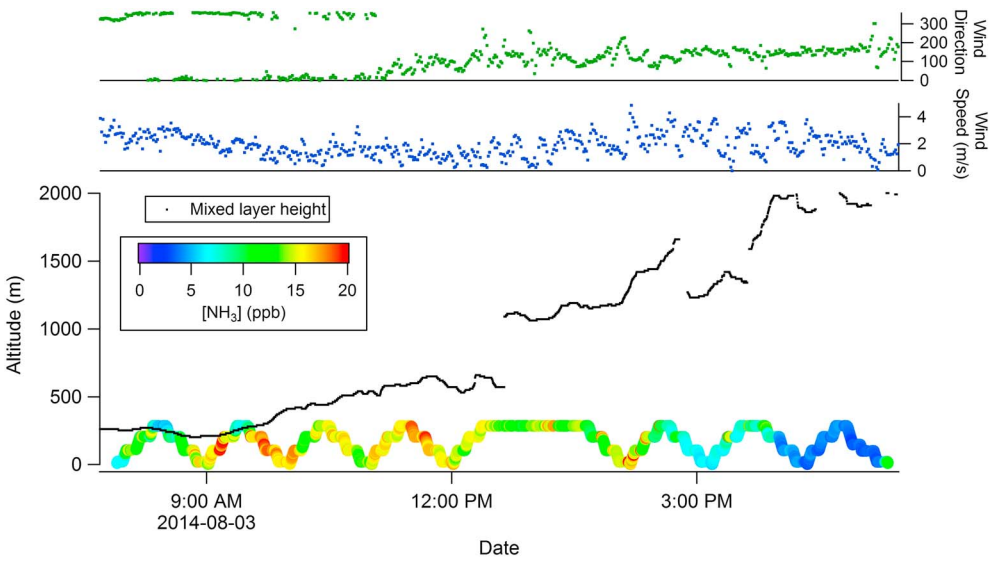

Figure 8. The bottom trace shows carriage altitude colored linearly by NH_3 mixing ratio. The black line shows the mixed layer height as measured by a ceilometer. The upper two traces show wind speed and wind direction measured on the tower at 100 m during the same time.

site (see section 4.1) (Li et al., 2016). The specific shape of these profiles is masked by the averaging used to generate Figure 4c and may explain the slightly lower mixing ratio observed at 10 m as compared to 100 m altitude (Figure 6). That the local surface sometimes acts as an NH_3 sink is to be expected given that the strongest sources impacting the location are at a distance from the measurement site. This leads to the occasional advection of NH_3-rich air masses over BAO, where surface equilibrium would suggest that deposition should occur (Zhang et al., 2010).

The observed relationships between NH_3 and meteorological variables in this data set are quite complex. With respect to gas-aerosol partitioning, high NH_3 mixing ratios are typically associated with high temperatures and low relative humidity, due to the influence of these factors on surface-atmosphere exchange and gas-particle partitioning (Gong et al., 2011; Lee et al., 1999; Li et al., 2014; Meng et al., 2011; Yamamoto et al., 1995). In this study, however, we see no relationship with temperature. This is not surprising given the low concentration of semivolatile NH_4NO_3 in this region, which minimizes the impact of temperature-driven gas-particle partitioning on gas-phase NH_3 mixing ratios. Particle NO_3^- measurements were made aboard several mobile platforms during this campaign, including by PILS-IC on the P3 aircraft. In order to ensure that the concentrations are as representative as possible, we select only data from time periods in which the aircraft was within 20 km of the BAO tower and under 280 m altitude, which gives a mean concentration of 1.04 $\mu g\ m^{-3}$ and a maximum value of 4.55 $\mu g\ m^{-3}$. As discussed previously, this suggests that volatilization of the NH_3 associated with this nitrate could typically contribute only approximately 0.3 ppb and, at the very most, 1.4 ppb NH_3. Based on this information, we infer that the gas-particle partitioning of NH_3 is likely responsible for, at most, sub-ppb level variation in the mixing ratios observed from the tower carriage.

Working opposite of the partitioning trend, however, emissions of NH_3 from CAFOs are observed to increase significantly throughout the day. This may be observed downwind of these sites if there is a strong enough temperature-driven increase in surface sources, along with enough turbulence that NH_3-rich air is transported to higher altitudes. Given that the measurement site itself is a less significant source of NH_3 than CAFOs to the north and east, the main meteorological driver appears to result from changes in wind direction rather than changes in temperature through their effects on emission strength. Additionally, since these more significant CAFO sources are located several kilometers away from the site, the impact of temperature on the strength of those particular surface sources will not be observed at the BAO site until the atmospheric transport of those air parcels from the northeast to the measurement site has occurred. This will likely cause some of the impacts of temperature to be observed some time after the temperature-driven emissions actually occur. A lack of positive correlation of NH_3 with temperature has been observed previously in similar locations surrounded by intensive agriculture where source region impacts dominate (Burkhardt et al., 1998; Chang et al., 2015; Horvath & Sutton, 1998; Pryor et al., 2001; Sharma et al., 2014; Vogt, Held, & Klemm, 2005).

3.2. Diurnal Trends

Figure 9a presents the NH_3 diurnal profile calculated for the entire column, while Figures 9b to 9d present the diurnal profiles at 280, 100, and 10 m, respectively. Corresponding diurnal profiles of temperature, wind speed, and relative humidity are shown in Figure S6. A comprehensive investigation of the relative importance of the individual and often opposing drivers of these diurnal trends is beyond the scope of the current work and would require detailed chemical transport modeling. We can, however, suggest some possible causes in the following section. At 100 and 280 m, NH_3 mixing ratios exhibit slight daytime maxima between approximately 8:00 and 16:00 MDT. The amplitude of these diurnal cycles, in terms of the ratio of the highest hourly mean to the lowest hourly mean, is slightly greater at 100 m (5.4) than 280 m (3.5). These diurnal patterns may be driven by horizontal transport and changing source regions. As seen in Figure 3b, wind direction at the site differs between night and daytime due to upslope and downslope flow. During the day, air is more likely to arrive from the northeast, where the majority of nearby CAFOs are located, whereas nighttime wind tends to arrive from the southwest, where there are fewer sources of NH_3. The transitions between these two airflow regimes happen between approximately 8:00 and 9:00 in the morning and between 15:00 and 21:00 in the evening. The timing of the daytime maxima in NH_3 mixing ratios at these two altitudes therefore coincides with the period of time during which they are influenced by higher NH_3 mixing ratios in air masses coming from the northeast.

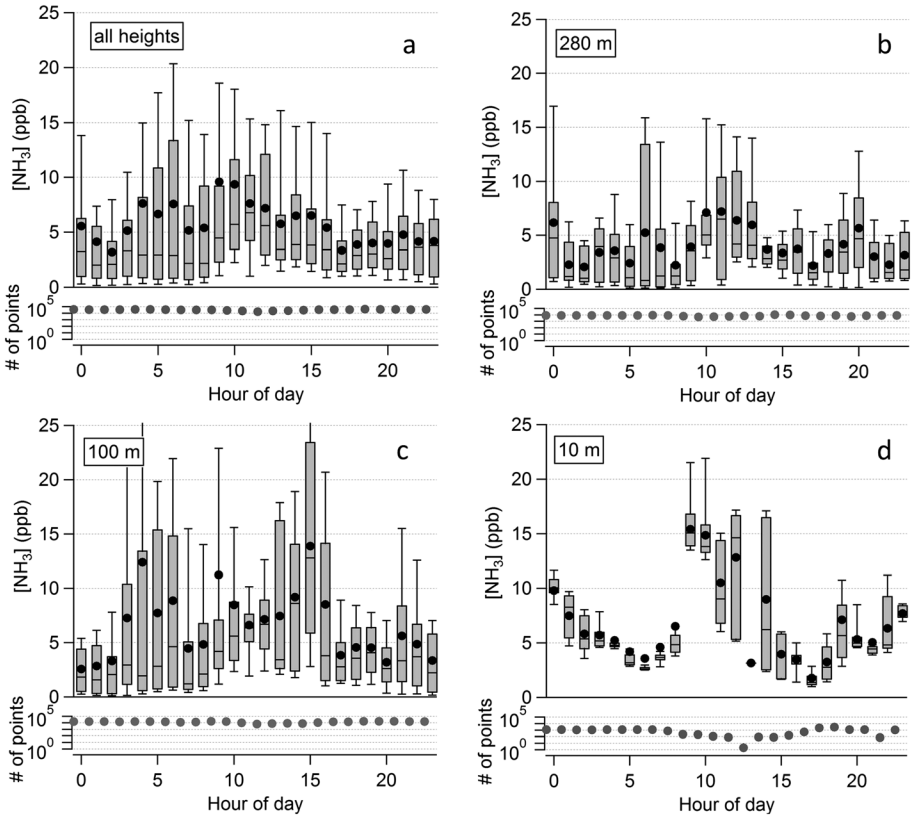

Figure 9. Diurnal profiles in NH_3 mixing ratios at three different measurement heights and throughout the column. The lines and dots represent the median and mean, respectively. The shaded boxes represent the 75th and 25th percentiles, while the whiskers represent the 90th and 10th percentiles. Also shown are the number of data points contained in each hourly bin.

At 10 m the mixing ratio increase during the day is sharper (amplitude ratio of 8.7), and begins earlier, with a slight increase at 7:00 MDT followed by a sharp increase between 8:00 and 9:00. There is also a small overnight peak at 10 m (increase 17:00–0:00 and decrease 0:00–7:00), which is absent at 100 m and 280 m. Since diurnal patterns in wind direction are relatively similar between the three stationary measurement heights (see Figure 3b), the differences in timing and amplitude of the daytime increase and the nocturnal peak at 10 m are not likely to be explained by differences in source region between altitudes. They might instead be due to the stronger influence of the local surface at this height, as well as the impacts of changing boundary layer height and mixing volume (Erisman et al., 2001; Fangmeier et al., 1994; Saylor et al., 2010). The increase between 8:00 and 9:00 may be due to the same change in source region that drives the daytime increase at 280 and 100 m. That the increase is sharper might be explained by greater proximity to the surface, where NH_3 mixing ratios are higher. The earlier increase in NH_3 mixing ratio (between approximately 6:00 and 8:00 MDT) could be driven by the impact of higher daytime temperature and wind speed and lower daytime relative humidity increasing the emission source strength of the local surface (Hatch, Jarvis, & Dollard, 1990; Hensen et al., 2009; Schjoerring, Husted, & Mattsson, 1998; Sutton et al., 2009; Wu et al., 2008). The average diurnal profile of temperature at this site (Figure S6) shows that the temperature at each height begins to increase around 6:00, along with a corresponding decrease in relative humidity. This is about an hour earlier than the initial increase in NH_3 at 10 m. Average wind speeds at 10 m, however, are at a minimum at this time of day, and this delay may therefore be due to the time required for the mixing ratio signal caused by this local temperature-driven increase in emission to be transported vertically. Vertical exchange velocity at this time of day was calculated following a simplified version of the resistance scheme of Hicks et al. (1987) and found to be approximately 0.5 cm s^{-1}. For the signal from a local temperature-driven emission increase in NH_3 to be transported to 10 m would therefore take about half an hour, which may help to explain the delay. Since the major CAFO sources of NH_3 are at a distance from the site, the impacts of

increasing temperature on the emission strength of these sources may also play a role in increasing NH_3 between 8:00 and 9:00 at 10 m, since it would take some time for this temperature-driven signal to arrive at the site. Taking an average wind speed at this time of 3 m s^{-1}, this 2 h delay between temperature change and mixing ratio change would be enough time for an air mass to move a distance of about 20 km, which is on the order of the distance between the measurement location and the more significant CAFO NH_3 sources to the northeast.

NH_3 mixing ratios can also vary with changes in the total mixing volume of the boundary layer (Fangmeier et al., 1994; Fowler et al., 2001; Saylor et al., 2010; Walker et al., 2006). The relatively rapid decrease in NH_3 at 10 m after 9:00 MDT may be due to the increase in mixed layer height between 9:00 and 13:00 (Figure S6), causing a dilution of surface NH_3. Wind speeds then continue to increase until about 16:00 (Figure S6), contributing to the more complete dilution of surface NH_3 throughout this mixed layer. The potential impact that dilution can have on daytime NH_3 mixing ratios may be seen in Figure 8. Here we see that between noon and 17:00 on the afternoon of 3 August, winds remain fairly constant while the mixed layer height increases fourfold, from approximately 500 to 2,000 m, and NH_3 mixing ratio decreases fivefold from 15 to 3 ppb. This observation suggests that dilution might account for some of the daytime decreases in NH_3 we measure at 10 m; however, more detailed chemical transport modeling would be needed to confirm this.

The increase at 10 m between 15:00 and 24:00 may be due to the increased emissions of NH_3 from the local surface once the mixing volume has stopped increasing and begins to collapse. This provides further evidence that the local surface can act as a source. Conversely, as discussed in section 3.2, the surface appears to act as an occasional nocturnal sink of NH_3. The decrease that begins around midnight despite the fairly constant reduced volume of the nighttime mixed layer over this time period may be due to the cooler surface beginning to act as a deposition sink. An estimate of flux (mixing ratio multiplied by previously calculated exchange velocity) gives a deposition rate at this time of day of about 20 ng m^{-2} s^{-1}. The decrease from midnight to 6:00 is on the order of 4 μg m^{-3} (or 6 ppb). Since this decrease occurs at 10 m but not at 100 m, we can calculate that the overall loss rate lies between 2 and 20 ng m^{-2} s^{-1} for mixing volumes that extend vertically to either 10 or 100 m. This flux is within the range calculated by bidirectional exchange models for this level of ambient NH_3 (e.g., Zhang et al., 2010) and suggests that deposition at this time may be rapid enough to account for the observed decrease in NH_3 over this time period.

Given the low concentration of semivolatile particle phase NH_4NO_3 in this region in summer measured previously (Day et al., 2012) and during this campaign (see section 3.1), temperature-driven gas-particle partitioning of NH_3 is unlikely to have a significant effect on mixing ratios. Since measured wind directions are similar at each height, the difference between the diurnal patterns may be impacted by the amount of influence that the surface has at each height. The differing degree of surface influence can be governed both by the distance of each measurement height from the surface and by whether the measurement height is above or below the boundary layer at any given time. The mixing ratio at 10 m is likely more strongly influenced by local surface impacts, which may cause its diurnal cycle to be of a greater amplitude, and more closely timed with the changes in meteorology that affect surface emissions. At higher altitudes, the impacts of changes in surface emissions are limited by the time needed to mix NH_3-rich air up through the column, and horizontal advection may play a greater role. Similarly, whereas the 10 m measurement height is impacted by the reduced mixing volume at night, the 100 m and 280 m boundary layer heights are often above the shallow nocturnal boundary layer and therefore do not experience the reduced mixing volume that may cause a nighttime increase in NH_3 at 10 m.

4. Literature Comparison and Discussion

4.1. Vertical Profiles

There have been relatively few measurements of the distribution of NH_3 within this vertical range of the atmosphere (Asman & van Jaarsveld, 1992; Erisman et al., 1988; Li et al., 2016). Previous measurements of NH_3 mixing ratios at nine altitudes on the BAO tower were made by Li et al. (2016) over the course of 1 year (Figure 10). Despite the use of the same measurement platform at the same location, the lower spatial resolution, as well as the longer sample integration time (2 weeks), and sampling period (1 year), make

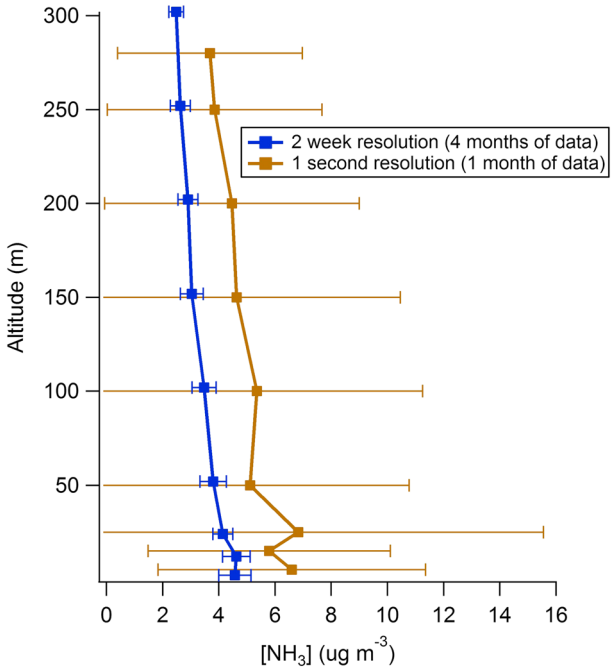

Figure 10. The blue traces show individual ~2 week average NH_3 concentrations measured by Li et al. (2016) in July and August of 2012 using passive samplers at nine heights on the BAO tower. The gold trace shows NH_3 concentrations measured by QC-TILDAS during the FRAPPÉ campaign averaged in 10 m bins around each of the heights at which the Li et al. (2016) samplers were deployed. The error bars represent standard deviation within each of these bins.

comparison with the FRAPPÉ observations difficult. In order to facilitate comparison, 10 m vertical segments were selected around each of the heights used by Li et al. (2016) and the FRAPPÉ campaign average within these segments was compared with average of Li et al. (2016) measurements over the same weeks for 2012. Both average profiles show an overall increase in NH_3 toward the surface. In the Li et al. (2016) profile this increase is smoother, likely because of the averaging effect of the longer time period over which the data were collected. The decrease in NH_3 at the lowest altitude seen in the average Li et al. (2016) profile is not reproduced in the average FRAPPÉ profile, although it was observed in some individual FRAPPÉ profiles (see section 3.2). Similarly, a number of individual Li et al. (2016) profiles do not show this decrease but increase continuously toward the surface. As discussed in section 3.2, this suggests that the surface at this site can act as either a source or sink, depending on conditions such as temperature and source region. The difference in the shapes of the two average profiles near to the surface may be due to differences in surface-atmosphere exchange between the 2 years. However, another issue in this comparison is that due to logistical limitations, the FRAPPÉ data set presented here is somewhat biased toward the daytime, when this surface decrease was not observed. Additionally, the mean night and day profiles correspond to a limited number of individual profiles. This is particularly true of nighttime profiles, which, because of logistical limitations during the campaign, are compiled from profiles during only two nights.

The overall increase in NH_3 concentrations toward the surface is also in agreement with some of the few other reports of measured vertical profiles of NH_3 at this scale, in observations made by Erisman et al. (1988) and by Asman and van Jaarsveld (1992), both at the same site in Netherlands. NH_3 mixing ratios were measured at four heights between the ground and 200 m, with a time resolution of two samples a day (9:00 to 21:00 and 21:00 to 9:00 local time). NH_3 mixing ratios were found to increase toward the ground with a smoother increase toward the surface than in the FRAPPÉ data set, though it may be possible to attribute this to the lower vertical resolution of their four heights (Erisman et al., 1988). The NH_3 gradient in the Erisman et al. (1988) study was found to be stronger during nighttime due to low turbulence and a shallower boundary layer. In contrast, closer to the ground (i.e., 0–200 cm) where surface emission strength would likely dominate over turbulence and boundary layer height, gradients have been found to be stronger in the daytime than at night (Hatch et al., 1990). It is difficult to determine whether nighttime or daytime gradients are stronger in the current study (see section 3.1), but both of these effects (higher daytime near-surface mixing ratios and lower turbulent-driven variability during the night) are evident.

There have been a number of examples of NH_3 observations from aircraft, providing information on the vertical distribution of NH_3 over an even wider vertical range (typically up to 5 or 6 km), though with less near-surface information. Over land, average NH_3 mixing ratios have been seen to decrease away from the surface, as expected for a compound with strong surface sources (Alkezweeny, Laws, & Jones, 1986; Georgii & Muller, 1974; Lebel et al., 1985; Leen et al., 2013; Nowak et al., 2010, 2012; Schiferl et al., 2014; Sun et al., 2015). Over areas with more of a tendency to act as a sink than a source (oceans for example), the opposite trend has been observed, with NH_3 mixing ratios increasing away from the surface (Lebel et al., 1985). Though the continental decrease in NH_3 with height is fairly consistently observed, there exists a lot of variability within these vertical profiles (Georgii & Muller, 1974; Lebel et al., 1985; Schiferl et al., 2014; Van Damme et al., 2015). This is likely due in part to the impacts of different source regions, as seen in this study. Boundary layer dynamics have an impact on the shape of the vertical profile over this spatial range because the isolation of higher altitudes from the influence of the surface leads to lower mixing ratios above the top of the well-mixed boundary layer (Georgii & Muller, 1974; Schiferl et al., 2014; Sun et al., 2015). Changes in boundary layer height may therefore also play a role in increasing the variability in NH_3 distribution. Though the height of the BAO tower

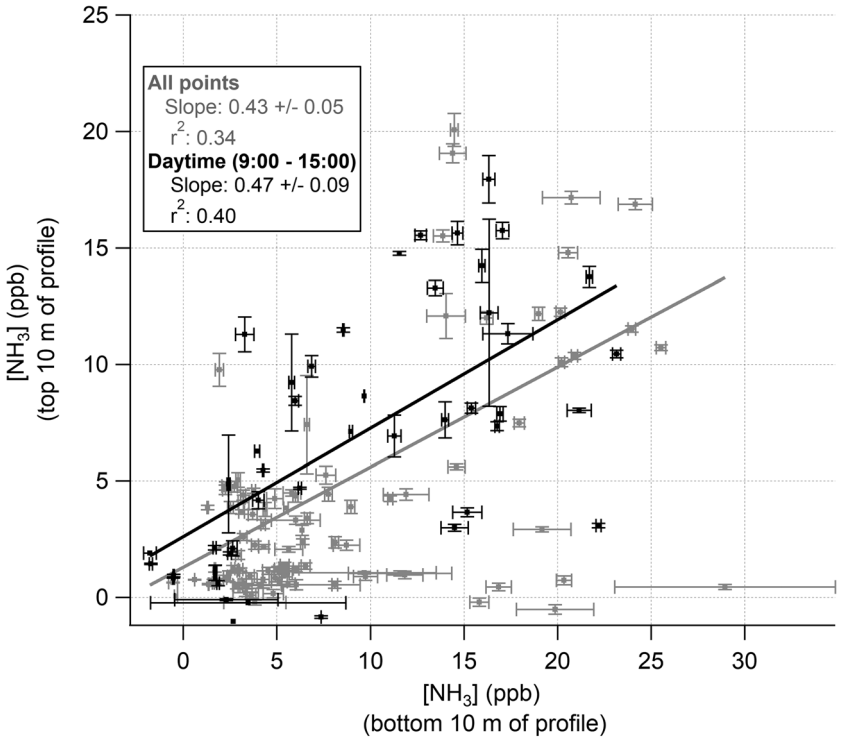

Figure 11. Correlation between average NH_3 mixing ratios in the top 10 and bottom 10 m of every individual profile. The black points show profiles measured during the daytime (between 9:00 and 15:00), while the grey points show all remaining profiles including those measured during the night and during transition times. The error bars show the standard deviation within each 10 m segment. The black line shows the linear best fit to the daytime data, while the grey line shows the linear best fit to all data, including daytime, nighttime, and transition times.

does not typically enable us to measure NH_3 above the daytime boundary layer, these aircraft observations are consistent with the decrease that we observe above the nighttime boundary layer at BAO.

Modeled vertical profiles over source regions tend to replicate the observed decrease of NH_3 with altitude (Schiferl et al., 2014; Shephard et al., 2011; Van Damme et al., 2014). These modeled profiles typically underestimate the observed mixing ratios of NH_3 from aircraft platforms, and this underestimate is largest near the surface (Lonsdale et al., 2016; Schiferl et al., 2014). Measurements from the BAO tower suggest that this underestimation may become more extreme even closer to the surface, as mixing ratios continue to increase toward the surface at altitudes below what can be measured from aircraft. Existing modeled and measured information on the vertical distribution of NH_3 has been essential for the determination of a priori profiles used in satellite retrievals of NH_3 mixing ratios, as well as the validation of these results (Lonsdale et al., 2016; Shephard et al., 2011; Shephard & Cady-Pereira, 2015; Sun et al., 2015; Van Damme et al., 2015; Warner et al., 2015). Retrievals are done using one of two or three different a priori profiles, depending on the amount of NH_3 present in the region under investigation. NH_3 mixing ratios in these a priori profiles typically increase toward the ground over polluted or moderately polluted regions, consistent with results found here (Shephard et al., 2011; Warner et al., 2015). The retrieved profile is highly sensitive to the shape and magnitude of the a priori profile (Shephard et al., 2011). More detailed information on the vertical distribution of NH_3, such as that presented in this paper, can therefore help to improve satellite retrievals in order to gain the benefits of the wider spatial and seasonal coverage that they offer. Figure 11 shows the correlation between the highest and lowest 10 m of every FRAPPÉ profile. The slope and r^2 value of the fit to all data (0.43 ± 0.05 and 0.34, respectively) show that while a relationship exists between ground-level mixing ratios and those measured aloft, the high degree of variability throughout the column causes the relationship to be quite weak. Even if the comparison is restricted to profiles measured during the daytime, when the boundary layer is expected to be well-mixed, the relationship is still quite weak (slope = 0.47 ± 0.09 and r^2 = 0.40). As discussed previously, this variability was seen to be strongly driven by source region, vertical mixing, and

boundary layer height. This result suggests that it is important to use caution in relating satellite and aircraft measurements to the composition of the air at ground level. Large near-surface changes in mixing ratio must be taken into account in developing and validating satellite algorithms, and even in assuming a well-mixed daytime boundary layer.

4.2. Diurnal Patterns

Diurnal patterns of NH_3 emissions reported in the literature are fairly consistent, showing increasing emissions during the day, driven by increasing temperature, wind speed, and animal activity, and decreasing relative humidity (Beauchamp, Kidd, & Thurtell, 1982; Flesch et al., 2007; Hatch et al., 1990; Hempel et al., 2016; Langford & Fehsenfeld, 1992; Ryden & Mcneill, 1984; Sutton et al., 2001). In contrast, there is a great deal of variability among observations of diurnal patterns of NH_3 mixing ratio. Some studies observe daytime increases in NH_3 mixing ratios, which can be explained by the increase in emission source strength with rising daytime temperatures (Asman & van Jaarsveld, 1992; Gong et al., 2011; Harrison & Allen, 1990; Langford & Fehsenfeld, 1992; Li, Schwab, & Demerjian, 2006; Nowak et al., 2006; Olszyna, Bairai, & Tanner, 2005; Phillips, Arya, & Aneja, 2004; Smith et al., 2007; Sutton et al., 2001; Wentworth et al., 2014). Others see nighttime maxima, which can be explained by accumulation of emissions within the reduced mixing volume of a shallow nighttime boundary layer (Burkhardt et al., 1998; Cadle, Countess, & Kelly, 1982; Erisman et al., 2001; Meng et al., 2011; Sakurai et al., 2003; Wyers, Otjes, & Slanina, 1993). Still others see an initial morning increase followed by a decrease in the afternoon, showing the interaction between these two drivers as the initial effect of increasing temperature-driven emissions is taken over by dilution effects (Georgii & Muller, 1974; Hu et al., 2008; Poulain et al., 2011; Trebs et al., 2005; Walker et al., 2006; Zhu et al., 2015). Similar variability can also be observed in modeling studies of diurnal NH_3 patterns (Asman & van Jaarsveld, 1992; Lonsdale et al., 2016; Pavlovic et al., 2006; Zhu et al., 2015).

Several previous analyses of the determinants of diurnal patterns have been carried out (Erisman et al., 2001; Fangmeier et al., 1994; Saylor et al., 2010). The determining factor in most cases seems to be not only the strength but also the location of the major source of NH_3 to the measurement location, in other words whether the local surface tends to act as a source or a sink. Erisman et al. (2001) and Saylor et al. (2010) suggest that daytime maxima tend to occur in remote regions, while in areas with high emissions, or at least with local sources, there tends to be a daytime minimum. As an explanation, Saylor et al. (2010) suggest that in areas of low emission, nighttime mixing ratios are depleted through deposition to the surface, leaving daytime emission to dominate, whereas in areas with local sources, mixing ratios can be replenished throughout the nighttime, and so the daytime dilution factor is more important. This trend is supported by most studies, with a few exceptions. Measurements that do not fit into this scheme, showing daytime maxima in areas with local sources tend to have either very high local emission sources, where the changes in emission source strength with temperature are presumably enough to overwhelm the dilution factor (Markovic et al., 2014; Phillips et al., 2004; Sun et al., 2015), or else are located in urban areas (Li et al., 2006; Nowak et al., 2006). In the case of the urban sites, it may be that either emission strength is strong enough to overwhelm dilution or that there is such an abundance of potential deposition surfaces that this process dominates.

One aspect that is not typically emphasized is the role of wind direction and air transport history in diurnal patterns (cf. Erisman et al., 2001; Gong et al., 2011; Sakurai et al., 2003). Because of the heterogeneity of source regions, this can have a significant impact, as seen in section 3.2. In the data set collected from the BAO tower, this seems to be the main factor driving the diurnal pattern at 100 and 280 m, since they are at such a distance from local surface influence. Because of this, the diurnal patterns at these two heights are less clearly influenced by the boundary layer height dilution effects and temperature-influenced emissions that impact diurnal patterns at many other sites. Our observations of the diurnal pattern at 10 m are more comparable to other studies, since they are at a more similar altitude. As mentioned in section 3.1, the local surface at this site can act as either a source or a sink, depending on the NH_3 mixing ratio of incoming air masses. As a result, we see both of the previously mentioned patterns; the site experiences maxima in mixing ratios both at night and during the daytime. Timing and temporal resolution complicate comparison with a previous observation of diurnal pattern in the region (Watson et al., 1998). Sampling from 6:00–12:00, 12:00–18:00, and 18:00–6:00 local time at a nearby site, Watson et al. (1998) observe slightly lower mixing ratios during the nighttime. When our data are averaged over the same time periods, however, we observe an afternoon, rather than a nighttime minimum

(Figure S7). This suggests that their measurement site becomes a stronger deposition sink earlier in the evening.

To our knowledge, only one other study has examined the difference in diurnal pattern with altitude. Wyers et al. (1993) made measurements at two points separated vertically by 10 m, with one above and one within the canopy. They observe the opposite change in diurnal pattern with height to what is observed here, with a daytime maximum at the lower measurement height (19 m), and a nighttime maximum at the higher measurement height (28 m). However, both of these altitudes are presumably located within the nocturnal boundary layer, and the influence of this reduced mixing volume can be seen in the 28 m nighttime maximum. The lower measurement height, on the other hand, is located within the canopy and may not experience the same boundary layer mixing as the other so that it may not experience the impact of this reduced volume. At the same time, its location within the canopy may magnify the influence of temperature-driven bidirectional exchange that would lead daytime emissions to dominate due to nighttime deposition.

These comparisons highlight the added complexity that measurement timing, location, and resolution (both spatial and temporal) can add to the interpretation of this data. Full column measurements at BAO, for example, might show different trends than the surface measurements made here, as seen in the difference between trends at individual heights and in the combination of all three heights. Similarly, the impact of short-term dramatic increases in mixing ratio from wind arriving from strong nearby point sources will have a different impact on the variability of biweekly as compared to 1 s measurements. The importance of timing can be seen in the way that some studies have found diurnal patterns to change throughout the year, exhibiting daytime minima in spring and winter, as compared to daytime maxima in the summer months (Khezri et al., 2013; Meng et al., 2011). Diurnal patterns at a given location can also change with meteorological conditions. This can be observed not only in the seasonal variation of diurnal patterns mentioned but also by filtering data with respect to various meteorological variables. Burkhardt et al. (1998), for example, observed a daytime maximum under high wind-speed conditions, whereas under low wind-speed conditions, daytime mixing ratios were at a minimum. Since NH_3 emissions tend to increase with wind speed, higher wind speeds presumably allow emission impacts to dominate over boundary layer effects (Sommer et al., 2009).

5. Conclusions

Based on this unique data set, two primary observations have been made. First, the mixing ratio of NH_3 during the summer at BAO tends to increase toward the surface. This appears to be driven by the lessening impact of the surface source at increasing altitude due to distance and the limitations of vertical exchange, as well as occasional isolation from the mixed layer. The high degree of variation between individual profiles is likely driven in part by changes in source region. This increasing trend is consistent with a previous measurement effort at this site (Li et al., 2016), except that we only see the decrease they observe at the very lowest (0–10 m) altitude in a few individual profiles and not in the average vertical trend. These occasional decreases, however, suggest that this surface can act as an occasional NH_3 sink as well as a source. The vertical information on NH_3 distribution presented here is particularly important given the need for accurate a priori profiles for developing satellite retrieval algorithms and for validating retrieval results. The large changes in NH_3 from 0 to 280 m might even need to be taken into consideration when assuming daytime boundary layers to be well-mixed.

Second, diurnal profiles of NH_3 at different altitudes were investigated for the first time and found to vary with measurement height. NH_3 mixing ratios at 280 m and 100 m show a slight midday increase, possibly driven by changes in source region caused by the transition between upslope and downslope flows. The patterns at 10 m are slightly more complicated and appear to be governed by the relative strengths of (1) changing emission source regions, (2) temperature-driven changes in emission, and (3) turbulence-driven changes in dilution volume. In order to push the interpretation of this data set further, a chemical transport model with a bidirectional surface flux scheme could be used to differentiate between the relative importance of these different and sometimes opposing drivers on the observed trends. This would require the characterization of the NH_3 emission potential at high spatial resolution, and ideally high time resolution, in the region around the site.

Acknowledgments
This work was supported by a Special Opportunity Graduate Travel Fellowship from the Department of Chemistry at the University of Toronto. Funding for Emily V. Fischer and many of the co-located observations collected at BAO during the FRAPPE period was provided by the Colorado Department of Public Health and Environment. Airborne PILS-IC data are provided by the NASA Langley Aerosol Research Group (Bruce Anderson and Andreas Beyersdorf) and were funded by NASA's Earth Venture-1 Program through the Earth System Science Pathfinder (ESSP) Program Office. PTR-ToF-MS measurements on the NASA P-3 were carried out by P. Eichler, T. Mikoviny, M. Müller, and A. Wisthaler and were supported by the Austrian Federal Ministry for Transport, Innovation and Technology (bmvit) through the Austrian Space Applications Programme (ASAP) of the Austrian Research Promotion Agency (FFG). The Princeton open-path NH3 measurements were conducted by K. Sun, L. Tao, D. Miller, D. Pan, L. Golston, L. Wendt, and M.A. Zondlo and supported by NASANNX14AT32G, NNX14AT36G, and NNX12AN64. The C-130 QC-TILDAS measurements were made by Rob Roscioli and Scott Herndon and were funded in part by the DOE SBIR Program (grant DESC0006193). Ceilometer data are provided by Travis Knepp and Jim Szykman from the National Aeronautics and Space Administration, with funding from the EPA National Exposure Research Laboratory. The authors gratefully acknowledge the contributions of Dan Wolfe, Dan Bon, William Dubé, Steve Brown, and members of the Delphine Farmer's Research Group for their help throughout the campaign and for useful discussions afterward. Data analysis was done in Igor Pro and R, using the packages openair and leaflet (Carslaw and Ropkins, 2012; R Core Team, 2016). Meteorological data from the Boulder Atmospheric Observatory are available at http://www.esrl.noaa.gov/psd/technology/bao. FRAPPE and DISCOVER-AQ data are available at http://www-air.larc.nasa.gov.

References

Adams, P. J., Seinfeld, J. H., Koch, D., Mickley, L., & Jacob, D. (2001). General circulation model assessment of direct radiative forcing by the sulfate-nitrate-ammonium-water inorganic aerosol system. *Journal of Geophysical Research*, *106*(D1), 1097–1111. https://doi.org/10.1029/2000JD900512

Alkezweeny, A. J., Laws, G. L., & Jones, W. (1986). Aircraft and ground measurements of ammonia in Kentucky. *Atmospheric Environment*, *20*(2), 357–360. https://doi.org/10.1016/0004-6981(86)90038-7

Aneja, V. P., Chauhan, J. P., & Walker, J. T. (2000). Characterization of atmospheric ammonia emissions from swine waste storage and treatment lagoons. *Journal of Geophysical Research*, *105*(D9), 11,535–11,545. https://doi.org/10.1029/2000JD900066

Aneja, V. P., Schlesinger, W. H., & Erisman, J. W. (2009). Effects of agriculture upon the air quality and climate: Research, policy, and regulations. *Environmental Science & Technology*, *43*(12), 4234–4240. https://doi.org/10.1021/es8024403

Asman, W. A. H., & van Jaarsveld, H. A. (1992). A variable-resolution transport model applied for NH_χ in Europe. *Atmospheric Environment*, *Part A, General Topics*, *26*(3), 445–464. https://doi.org/10.1016/0960-1686(92)90329-J

Atherton, E., Risk, D., Fougere, C., Lavoie, M., Marshall, A., Werring, J., … Minions, C. (2017). Mobile measurement of methane emissions from natural gas developments in northeastern British Columbia, Canada. *Atmospheric Chemistry and Physics*, *17*, 12,405–12,420. https://doi.org/10.5194/acp-17-12405-2017

Barthelmie, R. J., & Pryor, S. C. (1998). Implications of ammonia emissions for fine aerosol formation and visibility impairment—A case study from the lower Fraser Valley, British Columbia. *Atmospheric Environment*, *32*(3), 345–352. https://doi.org/10.1016/S1352-2310(97)83466-8

Beauchamp, E. G., Kidd, G. E., & Thurtell, G. (1982). Ammonia volatilization from liquid dairy cattle manure in the field. *Canadian Journal of Soil Science*, *19*, 11–19.

Benedict, K. B., Carrico, C. M., Kreidenweis, S. M., Schichtel, B., Malm, W. C., & Collett, J. L. (2013). A seasonal nitrogen deposition budget for Rocky Mountain National Park. *Ecological Applications*, *23*(5), 1156–1169. https://doi.org/10.1890/12-1624.1

Beyersdorf, A. J., Ziemba, L. D., Chen, G., Corr, C. A., Crawford, J. H., Diskin, G. S., & Moore, R. H. (2016). The impacts of aerosol loading, composition, and water uptake on aerosol extinction variability in the Baltimore-Washington, D. C. region. *Atmospheric Chemistry and Physics*, *16*(2), 1003–1015. https://doi.org/10.5194/acp-16-1003-2016

Brown, S. S., Thornton, J. A., Keene, W. C., Pszenny, A. A. P., Sive, B. C., Dubé, W. P., … Wolfe, D. E. (2013). Nitrogen, Aerosol Composition, and Halogens on a Tall Tower (NACHTT): Overview of a wintertime air chemistry field study in the front range urban corridor of Colorado. *Journal of Geophysical Research: Atmospheres*, *118*, 8067–8085. https://doi.org/10.1002/jgrd.50537

Burkhardt, J., Sutton, M. A., Milford, C., & Fowler, D. (1998). Ammonia concentrations at a site in southern Scotland from 2 yr of continuous measurements. *Atmospheric Environment*, *32*(3), 325–331. https://doi.org/10.1016/S1352-2310(97)00198-2

Cadle, S. H., Countess, R. J., & Kelly, N. A. (1982). Nitric acid and ammonia in urban and rural locations. *Atmospheric Environment*, *16*(10), 2501–2506. https://doi.org/10.1016/0004-6981(82)90141-X

Carslaw, D. C., & Ropkins, K. (2012). openair — An R package for air quality data analysis. *Environmental Modelling and Software*, *27–28*, 52–61. https://doi.org/10.1016/j.envsoft.2011.09.008

Chang, Y. H., Zou, Z., Deng, C. R., Huang, K., Collett, J. L., Lin, J., … Lin, J. (2015). The importance of vehicle emissions as a source of atmospheric ammonia in the megacity of Shanghai. *Atmospheric Chemistry and Physics Discussions*, *15*(23), 34,719–34,763. https://doi.org/10.5194/acpd-15-34719-2015

Chen, X., Day D., Schichtel B., Malm W., Matzoll A.K., Mojica J., … Collett Jr J.L. (2014). Seasonal ambient ammonia and ammonium concentrations in a pilot IMPROVE NHx monitoring network in the western United States. *Atmospheric Environment*, *91*, 118–126. https://doi.org/10.1016/j.atmosenv.2014.03.058

Day, D. E., Chen, X., Gebhart, K. A., Carrico, C. M., Schwandner, F. M., Benedict, K. B., … Collett, J. L. (2012). Spatial and temporal variability of ammonia and other inorganic aerosol species. *Atmospheric Environment*, *61*, 490–498. https://doi.org/10.1016/j.atmosenv.2012.06.045

Eilerman, S. J., Peischl, J., Neuman, J. A., Ryerson, T. B., Aikin, K. C., Holloway, M. W., … Herndon, S. (2016). Characterization of ammonia, methane, and nitrous oxide emissions from Concentrated Animal Feeding Operations in northeastern Colorado. *Environmental Science & Technology*, *50*(20), 10,885–10,893. https://doi.org/10.1021/acs.est.6b02851

Ellis, R. A., Murphy, J. G., Pattey, E., Van Haarlem, R., Brien, J. M. O., & Herndon, S. C. (2010). Characterizing a Quantum Cascade Tunable Infrared Laser Differential Absorption Spectrometer (QC-TILDAS) for measurements of atmospheric ammonia. *Atmospheric Measurement Techniques*, *3*(2), 397–406. https://doi.org/10.5194/amt-3-397-2010

Erisman, J. W., Bleeker, A., Galloway, J., & Sutton, M. S. (2007). Reduced nitrogen in ecology and the environment. *Environmental Pollution*, *150*(1), 140–149. https://doi.org/10.1016/j.envpol.2007.06.033

Erisman, J. W., Otjes, R., Hensen, A., Jongejan, P., van den Bulk, P., Khlystov, A., … Slanina, S. (2001). Instrument development and application in studies and monitoring of ambient ammonia. *Atmospheric Environment*, *35*(11), 1913–1922. https://doi.org/10.1016/S1352-2310(00)00544-6

Erisman, J.-W., Vermetten, A. W. M., Asman, W. A. H., Waijers-ijpelaan, A., & Slanina, J. (1988). Vertical distribution of gases and aerosols: The behaviour of ammonia and related components in the lower atmosphere. *Atmospheric Environment*, *22*(6), 1153–1160. https://doi.org/10.1016/0004-6981(88)90345-9

Fangmeier, A., Hadwiger-Fangmeier, A., Van DerEerden, L., & Jager, H.-J. (1994). Effects of atmospheric ammonia on vegetation—A review. *Environmental Pollution*, *86*(1), 43–82. https://doi.org/10.1016/0269-7491(94)90008-6

Fenn, M. E., Baron, J. S., Allen, E. B., Rueth, H. M., Nydick, K. R., Geiser, L., … Neitlich, P. (2003). Ecological effects of nitrogen deposition in the western United States. *Bioscience*, *53*(4), 404. https://doi.org/10.1641/0006-3568(2003)053%5B0404:EEONDI%5D2.0.CO;2

Flesch, T. K., Wilson, J. D., Harper, L. A., Todd, R. W., & Cole, N. A. (2007). Determining ammonia emissions from a cattle feedlot with an inverse dispersion technique. *Agricultural and Forest Meteorology*, *144*(1-2), 139–155. https://doi.org/10.1016/j.agrformet.2007.02.006

Fowler, D., Coyle, M., Flechard, C., Hargreaves, K., Nemitz, E., Sutton, M., & Erisman, J. (2001). Advances in micrometeorological methods for the measurement and interpretation of gas and particle nitrogen fluxes. *Plant and Soil*, *228*(1), 117–129. https://doi.org/10.1023/A:1004871511282

Gebhart, K. a., Schichtel, B. A., Malm, W. C., Barna, M. G., Rodriguez, M. A., & Collett, J. L. (2011). Back-trajectory-based source apportionment of airborne sulfur and nitrogen concentrations at Rocky Mountain National Park, Colorado, USA. *Atmospheric Environment*, *45*(3), 621–633. https://doi.org/10.1016/j.atmosenv.2010.10.035

Georgii, H. W., & Muller, W. J. (1974). On the distribution of ammonia in the middle and lower troposphere. *Tellus*, *26*(1970), 180–184.

Goebes, M. D., Strader, R., & Davidson, C. (2003). An ammonia emission inventory for fertilizer application in the United States. *Atmospheric Environment*, *37*(18), 2539–2550. https://doi.org/10.1016/S1352-2310(03)00129-8

Gong, L., Lewicki, R., Griffin, R. J., Flynn, J. H., Lefer, B. L., & Tittel, F. K. (2011). Atmospheric ammonia measurements in Houston, TX using an external-cavity quantum cascade laser-based sensor. *Atmospheric Chemistry and Physics*, *11*(18), 9721–9733. https://doi.org/10.5194/acp-11-9721-2011

Haagenson, P. L. (1979). Meteorological and climatological factors affecting Denver air quality. *Atmospheric Environment*, *13*(1), 79–85. https://doi.org/10.1016/0004-6981(79)90247-6

Harrison, R. M., & Allen, A. G. (1990). Measurements of atmospheric HNO3, HCl and associated species on a small network in eastern England. *Atmospheric Environment*, *24*(2), 369–376. https://doi.org/10.1016/0960-1686(90)90116-5

Hatch, D. J. J., Jarvis, S. C. C., & Dollard, G. J. (1990). Measurements of ammonia emission from grazed grassland. *Environmental Pollution*, *65*(4), 333–346. https://doi.org/10.1016/0269-7491(90)90125-V

Heald, C. L., Collett, J. L. Jr., Lee, T., Benedict, K. B., Schwandner, F. M., Li, Y., … Pye, H. O. T. (2012). Atmospheric ammonia and particulate inorganic nitrogen over the United States. *Atmospheric Chemistry and Physics*, *12*(21), 10,295–10,312. https://doi.org/10.5194/acp-12-10295-2012

Hempel, S., Kumer, C., Fiedler, M., Berg, W., Hansen, C., Amon, B., & Amon, T. (2016). Non-linear temperature dependency of ammonia and methane emissions from a naturally ventilated dairy barn. *Biosystems Engineering*, *145*, 10–21. https://doi.org/10.1016/j.biosystemseng.2016.02.006

Hensen, A., Loubet, B., Mosquera, J., van den Bulk, W. C. M., Erisman, J. W., Dämmgen, U., … Sutton, M. A. (2009). Estimation of NH3 emissions from a naturally ventilated livestock farm using local-scale atmospheric dispersion modelling. *Biogeosciences*, *6*(12), 2847–2860. https://doi.org/10.5194/bg-6-2847-2009

Henze, D. K., Shindell, D. T., Akhtar, F., Spurr, R. J. D., Pinder, R. W., Loughlin, D., … Shim, C. (2012). Spatially refined aerosol direct radiative forcing efficiencies. *Environmental Science & Technology*, *46*(17), 9511–9518. https://doi.org/10.1021/es301993s

Hicks, B. B., Baldocchi, D. D., Meyers, T. P., Hosker, R. P., & Matt, D. R. (1987). A preliminary multiple resistance routine for deriving dry deposition velocities from measured quantities. *Water, Air, and Soil Pollution*, *36*(3-4), 311–330. https://doi.org/10.1007/BF00229675

Horvath, L., & Sutton, M. A. (1998). Long-term records of ammonia and ammonium concentrations at K-Puszta, Hungary, *Atmos. Environment*, *32*(3), 339–344.

Hu, M., Wu, Z., Slanina, J., Lin, P., Liu, S., & Zeng, L. (2008). Acidic gases, ammonia and water-soluble ions in PM2.5 at a coastal site in the Pearl River Delta, China. *Atmospheric Environment*, *42*(25), 6310–6320. https://doi.org/10.1016/j.atmosenv.2008.02.015

Kaimal, J. C., & Gaynor, J. E. (1983). The Boulder Atmospheric Observatory. *Journal of Climate and Applied Meteorology*, *22*(5), 863–880. https://doi.org/10.1175/1520-0450(1983)022%3C0863:TBAO%3E2.0.CO;2

Khezri, B., Mo, H., Yan, Z., Chong, S.-L., Heng, A. K., & Webster, R. D. (2013). Simultaneous online monitoring of inorganic compounds in aerosols and gases in an industrialized area. *Atmospheric Environment*, *80*, 352–360. https://doi.org/10.1016/j.atmosenv.2013.08.008

Kljun, N., Calanca, P., Rotach, M. W., & Schmid, H. P. (2015). A simple two-dimensional parameterisation for Flux Footprint Prediction (FFP). *Geoscientific Model Development*, *8*(11), 3695–3713. https://doi.org/10.5194/gmd-8-3695-2015

Knepp, T. N., Szykman, J. S., Long, R., Duvall, R. M., Krug, J., Beaver, M., … Neil, D. (2017). Assessment of mixed-layer height estimation from single-wavelength ceilometer profiles. *Atmospheric Measurement Techniques Discussions*, *10*, 3963–3983. https://doi.org/10.5194/amt-10-3963-2017

Krupa, S. V. (2003). Effects of atmospheric ammonia (NH3) on terrestrial vegetation: A review. *Environmental Pollution*, *124*(2), 179–221. https://doi.org/10.1016/S0269-7491(02)00434-7

Langford, A. O., & Fehsenfeld, F. C. (1992). Natural vegetation as a source or sink for atmospheric ammonia: A case study. *Science*, *255*(5044), 581–583. https://doi.org/10.1126/science.255.5044.581

Lebel, P. J., Hoell, J. M., Levine, J. S., & Vay, S. A. (1985). Aircraft measurements of ammonia and nitric acid in the lower troposphere. *Geophysical Research Letters*, *12*(6), 401–404. https://doi.org/10.1029/GL012i006p00401

Lee, H. S., Kang, C., Kang, B.-W., & Kim, H.-K. (1999). Seasonal variations of acidic air pollutants in Seoul, South Korea. *Atmospheric Environment*, *33*(19), 3143–3152. https://doi.org/10.1016/S1352-2310(98)00382-3

Leen, J. B., Yu, X., Gupta, M., Baer, D. S., Hubbe, J. M., Kluzek, C. D., … Hubbell, M. R. (2013). Fast in situ airborne measurement of ammonia using a mid-infrared off-axis ICOS spectrometer. *Environmental Science & Technology*, *47*(18), 10,446–10,453. https://doi.org/10.1021/es401134u

Li, Y., Schwab, J. J., & Demerjian, K. L. (2006). Measurements of ambient ammonia using a tunable diode laser absorption spectrometer: Characteristics of ambient ammonia emissions in an urban area of New York City. *Journal of Geophysical Research*, *111*, D10S02. https://doi.org/10.1029/2005JD006275

Li, Y., Schwandner, F. M., Sewell, H. J., Zivkovich, A., Tigges, M., Raja, S., … Collett, J. L. Jr. (2014). Observations of ammonia, nitric acid, and fine particles in a rural gas production region. *Atmospheric Environment*, *83*(3), 80–89. https://doi.org/10.1016/j.atmosenv.2013.10.007

Li, Y., Thompson, T. M., van Damme, M., Chen, X., Benedict, K. B., Shao, Y., … Collett, J. L. Jr. (2016). Temporal and spatial variability of ammonia in urban and agricultural regions of northern Colorado, United States. *Atmospheric Chemistry and Physics*, *17*, 6197–6213. https://doi.org/10.5194/acp-17-6197-2017

Lonsdale, C. R., Hegarty, J. D., Alvarado, M. J., Henze, D. K., Turner, M. D., Vandenboer, T. C., … Scarino, A. J. (2016). Modeling the diurnal variability of agricultural ammonia in Bakersfield, California during the CalNex campaign. *Atmospheric Chemistry and Physics*, *17*, 2721–2739. https://doi.org/10.5194/acp-17-2721-2017

Markovic, M. Z., Vandenboer, T. C., Baker, K. R., Kelly, J. T., & Murphy, J. G. (2014). Measurements and modelling of the inorganic chemical composition of fine particulate matter and associated precursor gases in California's San Joaquin Valley during CalNex 2010. *Journal of Geophysical Research: Atmospheres*, *119*, 8201–8211. https://doi.org/10.1002/2013JD020063

McManus, J. B., Shorter, J. H., Nelson, D. D., Zahniser, M. S., Glenn, D. E., & McGovern, R. M. (2008). Pulsed quantum cascade laser instrument with compact design for rapid, high sensitivity measurements of trace gases in air. *Applied Physics B: Lasers and Optics*, *92*(3), 387–392. https://doi.org/10.1007/s00340-008-3129-9

Meng, Z. Y., Lin, W. L., Jiang, X. M., Yan, P., Wang, Y., Zhang, Y. M., … Yu, X. L. (2011). Characteristics of atmospheric ammonia over Beijing, China. *Atmospheric Chemistry and Physics*, *11*(12), 6139–6151. https://doi.org/10.5194/acp-11-6139-2011

Miller, D. J., Sun, K., Tao, L., Khan, M. A., & Zondlo, M. A. (2014). Open-path, quantum cascade-laser-based sensor for high-resolution atmospheric ammonia measurements. *Atmospheric Measurement Techniques*, *7*(1), 81–93. https://doi.org/10.5194/amt-7-81-2014

Moeckli, M. a., Fierz, M., & Sigrist, M. W. (1996). Emission factors for ethene and ammonia from a tunnel study with a photoacoustic trace gas detection system. *Environmental Science & Technology*, *30*(9), 2864–2867. https://doi.org/10.1021/es960152n

Müller, M., Mikoviny, T., Feil, S., Haidacher, S., Hanel, G., Hartungen, E., … Wisthaler, A. (2014). A compact PTR-ToF-MS instrument for airborne measurements of volatile organic compounds at high spatiotemporal resolution. *Atmospheric Measurement Techniques*, *7*(11), 3763–3772. https://doi.org/10.5194/amt-7-3763-2014

Neff, W. D. (2016). The Denver Brown cloud studies from the perspective of model assessment needs and the role of meteorology. *Journal of the Air & Waste Management Association (1995)*, *47*(3), 269–285. https://doi.org/10.1080/10473289.1997.10464447

Norman, M., Hansel, A., & Wisthaler, A. (2007). O2+ as reagent ion in the PTR-MS instrument: Detection of gas-phase ammonia. *International Journal of Mass Spectrometry*, *265*(2-3), 382–387. https://doi.org/10.1016/j.ijms.2007.06.010

Nowak, J. B., Huey, L. G., Russell, A. G., Tian, D., Neuman, J. A., Orsini, D., … Fehsenfeld, F. C. (2006). Analysis of urban gas phase ammonia measurements from the 2002 Atlanta Aerosol Nucleation and Real-Time Characterization Experiment (ANARChE). *Journal of Geophysical Research*, *111*, D17308. https://doi.org/10.1029/2006JD007113

Nowak, J. B., Neuman, J. A., Bahreini, R., Brock, C. A., Middlebrook, A. M., Wollny, A. G., … Fehsenfeld, F. C. (2010). Airborne observations of ammonia and ammonium nitrate formation over Houston, Texas. *Journal of Geophysical Research*, *115*, D22304. https://doi.org/10.1029/2010JD014195

Nowak, J. B., Neuman, J. A., Bahreini, R., Middlebrook, A. M., Holloway, J. S., McKeen, S. A., … Trainer, M. (2012). Ammonia sources in the California South Coast Air Basin and their impact on ammonium nitrate formation. *Geophysical Research Letters*, *39*, L07804. https://doi.org/10.1029/2012GL051197

Olszyna, K. J., Bairai, S. T., & Tanner, R. L. (2005). Effect of ambient NH3 levels on PM2.5 composition in the Great Smoky Mountains National Park. *Atmospheric Environment*, *39*(25), 4593–4606. https://doi.org/10.1016/j.atmosenv.2005.04.011

Pavlovic, R. T., Nopmongcol, U., Kimura, Y., & Allen, D. T. (2006). Ammonia emissions, concentrations and implications for particulate matter formation in Houston, TX. *Atmospheric Environment*, *40*, 538–551. https://doi.org/10.1016/j.atmosenv.2006.04.071

Phillips, S. B., Arya, S. P., & Aneja, V. P. (2004). Ammonia flux and dry deposition velocity from near-surface concentration gradient measurements over a grass surface in North Carolina. *Atmospheric Environment*, *38*(21), 3469–3480. https://doi.org/10.1016/j.atmosenv.2004.02.054

Phoenix, G. K., Emmett, B. A., Britton, A. J., Caporn, S. J. M., Dise, N. B., Helliwell, R., … Power, S. A. (2012). Impacts of atmospheric nitrogen deposition: Responses of multiple plant and soil parameters across contrasting ecosystems in long-term field experiments. *Global Change Biology*, *18*(4), 1197–1215. https://doi.org/10.1111/j.1365-2486.2011.02590.x

Pinder, R. W., Davidson, E. A., Goodale, C. L., Greaver, T. L., Herrick, J. D., & Liu, L. (2012). Climate change impacts of U.S. reactive nitrogen. *Proceedings of the National Academy of Sciences of the United States of America*, *109*(20), 7671–7675. https://doi.org/10.1073/pnas.1114243109

Pinder, R. W., Walker, J. T., Bash, J. O., Cady-Pereira, K. E., Henze, D. K., Luo, M., … Shephard, M. W. (2011). Quantifying spatial and seasonal variability in atmospheric ammonia with in situ and space-based observations. *Geophysical Research Letters*, *38*, L04802. https://doi.org/10.1029/2010GL046146

Poulain, L., Spindler, G., Birmili, W., Plass-Dülmer, C., Wiedensohler, A., & Herrmann, H. (2011). Seasonal and diurnal variations of particulate nitrate and organic matter at the IfT research station Melpitz. *Atmospheric Chemistry and Physics*, *11*(24), 12,579–12,599. https://doi.org/10.5194/acp-11-12579-2011

Pryor, S. C., Barthelmie, R. J., Sørensen, L. L., & Jensen, B. (2001). Ammonia concentrations and fluxes over a forest in the midwestern USA. *Atmospheric Environment*, *35*(32), 5645–5656. https://doi.org/10.1016/S1352-2310(01)00259-X

R Core Team (2016). *R: A language and environment for statistical computing*. R Foundation for Statistical Computing, Vienna. Retrieved from https://www.R-project.org/

Riedel, T. P., Wagner, N. L., Dubé, W. P., Middlebrook, A. M., Young, C. J., Öztürk, F., … Thornton, J. A. (2013). Chlorine activation within urban or power plant plumes: Vertically resolved ClNO 2 and Cl 2 measurements from a tall tower in a polluted continental setting. *Journal of Geophysical Research: Atmospheres*, *118*, 8702–8715. https://doi.org/10.1002/jgrd.50637

Ryden, J. C., & Mcneill, J. E. (1984). Application of the micrometeorological mass balance method to the determination of ammonia loss from a grazed sward. *Journal of the Science of Food and Agriculture*, *35*(12), 1297–1310. https://doi.org/10.1002/jsfa.2740351206

Sakurai, T., Fujita, S., Hayami, H., & Furuhashi, N. (2003). A case study of high ammonia concentration in the nighttime by means of modeling analysis in the Kanto region of Japan. *Atmospheric Environment*, *37*(31), 4461–4465. https://doi.org/10.1016/S1352-2310(03)00587-9

Saylor, R. D., Edgerton, E. S., Hartsell, B. E., Baumann, K., & Hansen, D. A. (2010). Continuous gaseous and total ammonia measurements from the southeastern aerosol research and characterization (SEARCH) study. *Atmospheric Environment*, *44*(38), 4994–5004. https://doi.org/10.1016/j.atmosenv.2010.07.055

Schiferl, L. D., Heald, C. L., Nowak, J. B., Holloway, J. S., Neuman, J. A., Bahreini, R., … Murphy, J. G. (2014). An investigation of ammonia and inorganic particulate matter in California during the CalNex campaign. *Journal of Geophysical Research: Atmospheres*, *119*, 1883–1902. https://doi.org/10.1002/2013JD020765

Schjoerring, J. K., Husted, S., & Mattsson, M. (1998). Physiological parameters controlling plant-atmosphere ammonia exchange. *Atmospheric Environment*, *32*(3), 491–498. https://doi.org/10.1016/S1352-2310(97)00006-X

Seinfeld, J. H., & Pandis, S. N. (2006). *Atmospheric chemistry and physics: From air pollution to climate change*. Hoboken, NJ: John Wiley.

Sharma, S. K., Mandal, T. K., Kumar, M., Gupta, N. C., Pathak, H., Harit, R. C., & Saxena, M. (2014). Measurement of ambient ammonia over the National Capital Region of Delhi, India. *Mapan-Journal Metrology Society of India*, *29*(3), 165–173. https://doi.org/10.1007/s12647-014-0098-9

Shephard, M. W., & Cady-Pereira, K. E. (2015). Cross-track Infrared Sounder (CrIS) satellite observations of tropospheric ammonia. *Atmospheric Measurement Techniques*, *8*(3), 1323–1336. https://doi.org/10.5194/amt-8-1323-2015

Shephard, M. W., Cady-Pereira, K. E., Luo, M., Henze, D. K., Pinder, R. W., Walker, J. T., … Clarisse, L. (2011). TES ammonia retrieval strategy and global observations of the spatial and seasonal variability of ammonia. *Atmospheric Chemistry and Physics*, *11*(20), 10,743–10,763. https://doi.org/10.5194/acp-11-10743-2011

Smith, A. M., Keene, W. C., Maben, J. R., Pszenny, A. A. P., Fischer, E., & Stohl, A. (2007). Ammonia sources, transport, transformation, and deposition in coastal New England during summer. *Journal of Geophysical Research*, *112*, D10S08. https://doi.org/10.1029/2006JD007574

Sommer, S. G., Christensen, B. T., & Nielsen, N. E. (1993). Ammonia volatilization during storage of cattle and pig slurry: Effect of surface cover. *The Journal of Agricultural Science*, *121*(01), 63–71. https://doi.org/10.1017/S0021859600076802

Sommer, S. G., Olesen, J. E., & Christensen, B. T. (2009). Effects of temperature, wind speed and air humidity on ammonia volatilization from surface applied cattle slurry. *The Journal of Agricultural Science*, *117*(01), 91. https://doi.org/10.1017/S0021859600079016

Stelson, A., & Seinfeld, J. (2007). Relative humidity and temperature dependence of the ammonium nitrate dissociation constant. *Atmospheric Environment*, *41*, 126–135. https://doi.org/10.1016/j.atmosenv.2007.10.063

Sun, K., Cady-Pereira, K., Miller, D. J., Tao, L., Zondlo, M. A., Nowak, J. B., … Hostetler, C. A. (2015). Validation of TES ammonia observations at the single pixel scale in the San Joaquin Valley during DISCOVER-AQ. *Journal of Geophysical Research: Atmospheres*, *120*, 5140–5154. https://doi.org/10.1002/2014JD022846

Sun, K., Tao, L., Miller, D. J., Khan, M. A., & Zondlo, M. A. (2014). On-road ammonia emissions characterized by mobile, open-path measurements. *Environmental Science & Technology*, *48*(7), 3943–3950. https://doi.org/10.1021/es4047704

Sun, K., Tao, L., Miller, D. J., Pan, D., Golston, L. M., Zondlo, M. A., … Zhu, T. (2017). Vehicle emissions as an important urban ammonia source in the United States and China. https://doi.org/10.1021/acs.est.6b02805

Sun, K., Tao, L., Miller, D. J., Zondlo, M. A., Shonkwiler, K. B., Nash, C., & Ham, J. M. (2015). Open-path eddy covariance measurements of ammonia fluxes from a beef cattle feedlot. *Agricultural and Forest Meteorology*, *213*, 193–202. https://doi.org/10.1016/j.agrformet.2015.06.007

Sutton, M. A., Milford, C., Nemitz, E., Theobald, M. R., Hill, P. W., Fowler, D., … Riedo, M. (2001). Biosphere-atmosphere interactions of ammonia with grasslands: Experimental strategy and results from a new European initiative. *Plant and Soil*, *228*(1), 131–145. https://doi.org/10.1023/A:1004822100016

Sutton, M. A., Nemitz, E., Milford, C., Campbell, C., Erisman, J. W., Hensen, A., … Burkhardt, J. (2009). Dynamics of ammonia exchange with cut grassland: Synthesis of results and conclusions of the GRAMINAE Integrated Experiment. *Biogeosciences*, *6*(12), 2907–2934. https://doi.org/10.5194/bg-6-2907-2009

Toth, J., Toth, J., & Johnson, R. H. (1984). Summer surface flow characteristics over Northeast Colorado. *Monthly Weather Review*, *113*, 1458–1469.

Trebs, I., Metzger, S., Meixner, F. X., Helas, G., Hoffer, A., Rudich, Y., … Andreae, M. O. (2005). The NH4+ NO3−Cl−SO42−H2O aerosol system and its gas phase precursors at a pasture site in the Amazon Basin: How relevant are mineral cations and soluble organic acids? *Journal of Geophysical Research*, *110*, D07303. https://doi.org/10.1029/2004JD005478

Van Damme, M., Clarisse, L., Dammers, E., Liu, X., Nowak, J. B., Clerbaux, C., … Coheur, P. F. (2015). Towards validation of ammonia (NH3) measurements from the IASI satellite. *Atmospheric Measurement Techniques*, *8*(3), 1575–1591. https://doi.org/10.5194/amt-8-1575-2015

Van Damme, M., Clarisse, L., Heald, C. L., Hurtmans, D., Ngadi, Y., Clerbaux, C., … Coheur, P. F. (2014). Global distributions, time series and error characterization of atmospheric ammonia (NH3) from IASI satellite observations to cite this version. *Atmospheric Chemistry and Physics*, *14*, 2905–2922.

Vogt, E., Held, A., & Klemm, O. (2005). Sources and concentrations of gaseous and particulate reduced nitrogen in the city of Münster (Germany). *Atmospheric Environment*, *39*(38), 7393–7402. https://doi.org/10.1016/j.atmosenv.2005.09.012

Walker, J. T., Whitall, D. R., Robarge, W., & Paerl, H. W. (2004). Ambient ammonia and ammonium aerosol across a region of variable ammonia emission density. *Atmospheric Environment*, *38*(9), 1235–1246. https://doi.org/10.1016/j.atmosenv.2003.11.027

Walker, J. T. T., Robarge, W. P. P., Wu, Y., & Meyers, T. P. P. (2006). Measurement of bi-directional ammonia fluxes over soybean using the modified Bowen-ratio technique. *Agricultural and Forest Meteorology*, *138*(1-4), 54–68. https://doi.org/10.1016/j.agrformet.2006.03.011

Warner, J. X., Wei, Z., Strow, L. L., Dickerson, R. R., & Nowak, J. B. (2015). The global tropospheric ammonia distribution as seen in the 13 year AIRS measurement record. *Atmospheric Chemistry and Physics Discussions*, *15*(24), 35,823–35,856. https://doi.org/10.5194/acpd-15-35823-2015

Watson, J. G., Nv, R., Richards, L. W., & Neff, W. (1998). Northern Front Range air quality study final report.

Wentworth, G. R., Murphy, J. G., Gregoire, P. K., Cheyne, C. A. L., Tevlin, A. G., & Hems, R. (2014). Soil-atmosphere exchange of ammonia in a non-fertilized grassland: Measured emission potentials and inferred fluxes. *Biogeosciences*, *11*(20), 5675–5686. https://doi.org/10.5194/bg-11-5675-2014

Wu, S.-Y., Hu, J.-L., Zhang, Y., & Aneja, V. P. (2008). Modeling atmospheric transport and fate of ammonia in North Carolina—Part II: Effect of ammonia emissions on fine particulate matter formation. *Atmospheric Environment*, *42*(14), 3437–3451. https://doi.org/10.1016/j.atmosenv.2007.04.022

Wyers, G. P., Otjes, R. P., & Slanina, J. (1993). A continuous-flow denuder for the measurement of ambient concentrations and surface-exchange fluxes of ammonia. *Atmospheric Environment*, *27*(13), 2085–2090. https://doi.org/10.1016/0960-1686(93)90280-C

Yamamoto, N., Nshiura, H., Honjo, T., Ishikawa, Y., & Suzuki, K. (1995). A long-term study of atmospheric ammonia and particulate ammonium concentrations in Yokohama, Japan. *Atmospheric Environment*, *29*(1), 97–103. https://doi.org/10.1016/1352-2310(94)00226-B

Zhang, L., Wright, L. P., & Asman, W. A. H. (2010). Bi-directional air-surface exchange of atmospheric ammonia: A review of measurements and a development of a big-leaf model for applications in regional-scale air-quality models. *Journal of Geophysical Research*, *115*, D20310. https://doi.org/10.1029/2009JD013589

Zhu, L., Henze, D. K., Bash, J. O., Cady-Pereira, K. E., Shephard, M. W., Luo, M., & Capps, S. L. (2015). Sources and impacts of atmospheric NH3: Current understanding and Frontiers for modeling, measurements, and remote sensing in North America. *Current Pollution Reports*, *1*(2), 95–116. https://doi.org/10.1007/s40726-015-0010-4